HHS Public Access

Author manuscript

*Cell Metab*. Author manuscript; available in PMC 2020 February 05.

Published in final edited form as:

*Cell Metab*. 2019 February 05; 29(2): 417–429.e4. doi:10.1016/j.cmet.2018.10.013.

# Quantitative analysis of the whole-body metabolic fate of branched chain amino acids

**Michael D. Neinast**[#1], **Cholsoon Jang**[#1,2], **Sheng Hui**[2], **Danielle S. Murashige**[1], **Qingwei Chu**[1], **Raphael J. Morscher**[2], **Xiaoxuan Li**[2], **Le Zhan**[3], **Eileen White**[3], **Tracy G. Anthony**[4], **Joshua D. Rabinowitz**[2], and **Zoltan Arany**[1,#]

[1]Perelman School of Medicine, University of Pennsylvania, 3400 Civic Blvd, Philadelphia, PA USA 19104

[2]Department of Chemistry and Lewis-Sigler Institute for Integrative Genomics, Princeton University, Princeton, NJ USA 08544

[3]Rutgers Cancer Institute of New Jersey, New Brunswick, NJ USA 08903

[4]Department of Nutritional Sciences and the New Jersey Institute for Food, Nutrition and Health, Rutgers University, New Brunswick, NJ USA 08901

[#] These authors contributed equally to this work.

## Abstract

Elevations in branched-chain amino acids (BCAAs) associate with numerous systemic diseases, including cancer, diabetes, and heart failure. However, an integrated understanding of whole-body BCAA metabolism remains lacking. Here, we employ *in vivo* isotopic tracing to systemically quantify BCAA oxidation in healthy and insulin resistant mice. We find that most tissues rapidly oxidize BCAAs into the TCA cycle, with the greatest quantity occurring in muscle, brown fat, liver, kidneys and heart. Notably, pancreas supplies 20% of its TCA carbons from BCAAs. Genetic and pharmacologic suppression of BCKDK, a clinically targeted regulatory kinase, induces BCAA oxidation primarily in skeletal muscle of healthy mice. While insulin acutely increases BCAA oxidation in cardiac and skeletal muscle, chronically insulin-resistant mice show blunted BCAA oxidation in adipose tissues and liver, shifting BCAA oxidation toward muscle. Together, this work provides a quantitative framework for understanding systemic BCAA oxidation in health and insulin resistance.

## Graphical Abstract

[#]Correspondence and lead contact: zarany@pennmedicine.upenn.edu (Z.A).

AUTHOR CONTRIBUTIONS

M.D.N., C.J., J.D.R., and Z.A. designed the study. M.D.N., and C.J. performed most experiments. S.H., C.J., R.J.M., X.L., and J.D.R. performed mass spectrometry and contributed to data analysis. D.S.M. contributed to design and execution of the BT2 study and contributed to the heat map of gene expression and western blots. Q.C. and L.Z. performed catheter placement surgery and infusions. C.J., L.Z., E.W., and T.G.A designed and performed the BCKDK KO mouse studies. M.D.N., C.J., S.H., J.D.R., and Z.A. developed the model of whole-body BCAA oxidation. M.D.N., C.J., and Z.A. wrote the manuscript. All authors discussed the results and commented on the manuscript.

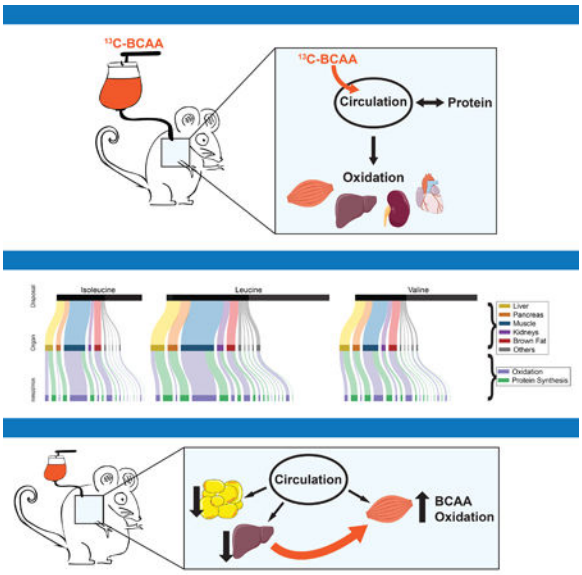


## Abstract

Increases in branched-chain amino acids (BCAAs) has been associated with diabetes, cancer and heart failure. Here, XXX et al use *in vivo* isotopic tracing to provide an integrated overview of whole-body BCAA metabolism. A shift in BCAA oxidation away from adipocytes and liver, towards muscle, is seen in insulin resistance.

## INTRODUCTION

Reports since the 1960s have noted that elevations in circulating BCAAs tightly associate with insulin resistance (Felig et al., 1969), and more recent studies have also found associations with pancreatic cancer and heart disease (Huang et al., 2011; Mayers et al., 2014). Metabolomics profiling in large prospective epidemiological studies have shown that serum elevations in BCAAs predict insulin resistance and diabetes as much as 20 years prior to clinical presentation, and a decade before any other known marker or test (Wang et al., 2011). Feeding rodents a diabetogenic diet supplemented with BCAAs markedly worsens the ensuing insulin resistance (Newgard et al., 2009). Most recently, a human Mendelian randomization study demonstrated that polymorphisms that cause elevations in BCAAs also predict insulin resistance (Lotta et al., 2016). Together, these studies demonstrate with near-certainty that aberrant metabolism of BCAAs contributes to insulin resistance in humans. Conversely, insulin resistance may also promote BCAA accumulation (Wang et al., 2017; Mahendran et al., 2017), potentially leading to a vicious cycle. The mechanisms behind these causal maladaptive metabolic disturbances remain unexplained, a gap that in large part reflects a still limited understanding of system-wide handling of BCAA metabolism.

The three BCAAs (leucine, valine, and isoleucine) are essential amino acids and abundant, accounting for ~35% of essential amino acids and ~21% of total amino acids in muscle protein (Harper et al., 1984). The small size and hydrophobicity of BCAAs provide indispensable structural properties for proteins. In addition, BCAAs and their metabolic

products can act as molecular signals: for example, leucine activates the mTORC1 pathway (Anthony et al., 2000), and metabolites of valine oxidation, beta-aminoisobutyric acid (BAIBA) and 3-hydroxyisobutyrate (3-HIB), induce browning of white fat and trans-endothelial fatty acid transport, respectively (Roberts et al., 2014; Jang et al., 2016). Understanding the role of BCAAs in insulin resistance and other pathologies thus requires an understanding of BCAA metabolism, both biochemically and at the whole-body level.

Biochemically, BCAA metabolism is relatively well described. The initial steps of BCAA metabolism are shared: all three BCAAs first undergo transamination by branched chain aminotransferases (BCATs) to form branched chain alpha-ketoacids (BCKAs), which then can undergo irreversible oxidative decarboxylation by the mitochondrial branched chain alpha-ketoacid dehydrogenase (BCKDH) complex (Brosnan and Brosnan, 2006). BCKDH also simultaneously traps inside the mitochondria all intermediate metabolites, with the exception of 3-HIB, by adding a bulky and hydrophilic co-enzyme A (CoA) adduct. This flux-controlling step is a critical point of regulation: nutrition, exercise, and hormones can modulate BCAA metabolism via BCKDH kinase (BCKDK), which phosphorylates the E1α subunit of BCKDH (BCKDHA) to inhibit activity. Conversely, protein phosphatase-2Cm removes this phosphorylation to promote BCKDH activity (Lu et al., 2009). The catabolic steps of each of the three BCAAs differ after oxidation by the BCKDH complex. However, because BCKDH catalyzes the flux-controlling step, the rates of oxidation for all three BCAAs are linked. Ultimately, carbons that stem from BCAA catabolism enter the TCA cycle as either acetyl-CoA or succinyl-CoA, where they can then be completely oxidized.

At the whole-body level, in contrast, BCAA metabolism is less well understood. The circulating pool of free BCAAs is determined by a balance between input (e.g., diet, proteolysis) and output (e.g., protein synthesis, catabolism for energy). Dietary BCAAs are initially taken up with other nutrients by the intestine, but unlike other amino acids, a majority of BCAAs bypass “first pass” hepatic metabolism, likely in part due to the relatively low transamination activity of hepatocytes in the liver (Hutson et al., 1992). Some transamination likely does occur in the liver, as BCAT is present in non-hepatocyte cells in the liver (Ding et al., 2016), but how much is not clear. Extrahepatic tissues transaminate most BCAAs and can return their cognate alpha-ketoacids to the liver for oxidation by BCKDH (Goodwin et al., 1998; Shin et al., 2014). BCKDH, however, is also expressed and active in most tissues including muscle, white adipose, kidney, and brain (Suryawan et al., 1998; Brosnan and Brosnan, 2006; Herman et al., 2010). How whole-body BCAA oxidation is partitioned has been inconclusive. Previous reports rely on *ex vivo* measurements of isolated enzymes or explanted tissues, sometimes perfused and sometimes not (Goodwin et al., 1998; Suryawan et al., 1998; Herman et al., 2010; Tso et al., 2014; Shin et al., 2014), and thus cannot address actual metabolic flux *in vivo*. Accordingly, the quantitative significance of inter-organ exchange of BCAA metabolites, the relative contributions of each tissue to whole-body BCAA oxidation, and how these processes are altered in pathological states *in vivo* remain unclear.

Here we utilized isotope tracers and metabolomics to systemically analyze whole-body BCAA metabolism in conscious animals. We found remarkable differences in BCAA oxidation among individual organs, and alterations in their contribution to systemic

oxidation in response to insulin and in states of insulin resistance. We also quantified tissue-specific regulation of BCAA oxidation using genetic and pharmacological intervention. This work provides quantitative insights on the dynamics of systemic BCAA metabolism and highlights the value of isotopetracer studies to investigate macronutrient homeostasis at the whole-body level.

## RESULTS

### Multiple tissues oxidize BCAAs quickly.

BCAAs share the first two steps of oxidation, catalyzed by BCAT and BCKDH, after which the carbons of BCAA oxidation ultimately enter the TCA cycle (Figure 1A). To assess the early systemic kinetics of BCAA oxidation, we injected mice intravenously with BCAAs (one labeled with $^{13}C$ and the other two unlabeled), and collected blood and tissues at different time points for metabolite measurement by mass spectrometry (Figure 1B). After the initial bolus-induced rise, circulating levels of BCAAs quickly dropped (half-life ~4 minutes), while levels of BCKAs and 3-HIB concomitantly rose (Figures 1C, S1A, S1F). Within 60 seconds, $^{13}C$-labeling of circulating BCKAs reached ~50% that of BCAAs, indicating extremely fast transamination (Figures 1D, S1B, S1G). Strikingly, we also saw significant labeling (~20%) of circulating 3-HIB within just three minutes. Thus, the process of tissue uptake of valine, oxidation to 3-HIB (which involves 6 enzymatic reactions in mitochondria), and release of 3-HIB back into circulation, required less than 3 min (Figure 1D). We did not see significant labeling of the TCA intermediate succinate in circulation within this timeframe (Figures 1D, S1B, S1G). Thus, BCAA catabolism is rapid *in vivo*.

What tissues metabolize BCAAs this quickly? Published gene expression databases suggest the potential for BCAA oxidation capacity in numerous tissues (Figure S1K). To identify tissues capable of rapid BCAA oxidation, we tracked the kinetics of $^{13}C$-labeling in BCAA metabolites after a bolus delivery of $^{13}C$-labeled BCAAs. Labeled BCAAs were found in all tissues collected, indicating rapid tissue uptake and equilibration of BCAAs (Figures 1E, S1C, and S1H). BCKAs labeling was higher than in blood in all tissues except for the liver, indicating rapid transamination system-wide (Figures 1F, S1D, and S1I). Labeled 3-HIB was also markedly higher in all tissues than in blood, demonstrating functional BCKDH activity and subsequent production of 3-HIB in all of these tissues (Figure 1G). Even when succinate labeling in plasma was undetectable, we found significant labeling in succinate in all tissues – clearly demonstrating BCAA oxidation occurring in these tissues (Figures 1H, S1E, and S1J). Interestingly, BCAA oxidation was particularly pronounced in the pancreas (Figures 1F-1H, S1E, and S1J). Thus, we conclude that most tissues actively oxidize all three BCAAs.

### Quantitative analysis of whole-body BCAA oxidation

The above experiments indicated that many tissues oxidize BCAAs. However, a rigorous comparison of oxidation in different tissues is difficult because the kinetics of BCAA transport and oxidation likely differ between tissues. Moreover, the relatively large bolus of BCAAs may perturb the system, e.g. by activating BCKDH (Lau et al., 1982). We therefore performed a series of constant infusions with a small amount of all three BCAAs, in each

case with one of the BCAAs universally labeled with $^{13}C$ (Figure 2A). These infusions achieved steady-state labeling of circulating BCAA within 120 minutes (Figure 2B, S2B, and S2C) with a modest (~1.3x) increase in their total pool size (Figure S2A), a perturbation similar to feeding (Jeyaraj D et al., 2012). In the $^{13}C$-valine infusion, the labeling of circulating αKIV and 3-HIB also reached similar labeling (~15-18%) (Figure S2D), suggesting that most circulating 3-HIB is derived from valine, rather than other proposed precursors such as thymine (Marcadier et al., 2013). From the % labeling and our known infusion rate for each $^{13}C$-BCAA, we calculated the rate of appearance ($R_a$) of total endogenous (unlabeled) BCAAs at 845 nmoles/min for a 25g mouse. The calculated $R_a$ of each individual BCAA correlated perfectly with the concentrations of each BCAA in proteins (Figure 2C and Davis et al., 1994), consistent with the source of circulating BCAAs being proteolysis. Over 24 hours, such a rate yields 154 mg of BCAAs, approximately matching the daily dietary intake of 164 mg of BCAAs, assuming ~4 grams of chow consumed per day (LabDiet 5001, Bachmanov et al., 2002). This suggests that the $R_a$ of BCAAs may remain relatively stable throughout the 24-hour cycle to maintain systemic homeostasis during the fed/fasted cycle (Jeyaraj et al., 2012).

At steady-state homeostasis, BCAAs released from proteins must be either oxidized or reused for protein synthesis. We first evaluated tissue BCAA oxidation flux by measuring in various tissues $^{13}C$ labeling of TCA intermediates during infusion with each BCAA tracer. We quantified the fraction of $^{13}C$ labeling in all isotopomers (M+1, M+2, etc) of succinate or malate, the two most abundant TCA intermediates, and normalized this total $^{13}C$ labeling to that in the circulating BCAA being evaluated (Hui et al., 2018). Labeling of the TCA intermediates from BCAAs reached steady-state within 120 minutes of infusion (Figure S2E) and markedly differed between tissues (Figure 2D). Most tissues used BCAA carbons to supply 1-6% of carbons in the TCA cycle, while the pancreas was unique in that it used BCAA carbons to supply ~20% of the TCA carbons (Figure 2D). A negligible portion of this TCA labeling stems from indirect oxidation of mildly labeled circulating glucose, lactate or glutamine, as calculated by simple matrix equations (Figures S2F and S2G) (Hui et al., 2018). Similarly, steady-state $^{13}C$-αKIV infusion indicated that $R_a$ of αKIV is only <25% that of valine (Figures S2H-S2J), with concomitant low contribution of carbons to TCA cycle in most organs (Figure S2K), indicating that the majority of TCA labeling from BCAAs is through direct oxidation of BCAAs in individual tissues rather than indirect oxidation of circulating BCKAs.

This quantification of tissue preference for BCAA carbons in the TCA cycle can be used to estimate BCAA oxidation flux. Assuming the rate that carbons enter and leave the TCA cycle (TCA turnover, $J_{TCA}$) is at steady state, the flux of BCAA carbon entry (BCAA oxidation, $J_{BCAA\ ox}$) is equal to the TCA turnover times the fraction of TCA carbons derived from BCAA ($f_{BCAA/TCA}$).

$$J_{BCAA\ ox} = J_{TCA} * f_{BCCAA/TCA}$$

For example, even though BCAA contribution to the TCA is high in the pancreas, the TCA turnover in the pancreas is lower than highly metabolically active tissues like the heart. We

thus combined our measured $f_{BCAA/TCA}$ (Figure 2D and Table S1), with published values of tissue oxygen consumption to approximate $J_{TCA}$(Table S2, Randle et al., 1970; Malloy et al., 1996), to estimate the tissue BCAA oxidation flux (Figure 2E). The heart and brown fat showed the highest BCAA oxidation flux (per g tissue) followed by pancreas and kidneys (Figure 2F). Of note, these measured rates of oxidation could not have been predicted by BCKDHA mRNA expression in those tissues (Figure 2G).

We next evaluated BCAA disposal rates into protein synthesis, by measuring incorporation of $^{13}$C-leucine into proteins in each tissue during steady-state $^{13}$C-leucine infusion. Assuming that the protein in a given tissue is a single well-mixed pool and protein synthesis rate is the same for the entire organ, the fractional rate of protein synthesis (FSR) can be used to calculate the rate of BCAA disposal into protein synthesis:

$$\frac{fraction\ synthesized}{minute} * \frac{g\ protein}{g\ tissue} * \frac{mol\ BCCA}{g\ protein} = \frac{mol\ BCAA}{minute\ *\ g\ tissue}$$

Strikingly, the pancreas again showed a uniquely high FSR (Figure 2H) and rate of BCAA disposal into protein synthesis (Figure 2I), mirroring its high BCAA usage for the TCA cycle (Figure 2D). We did not, however, observe a general correlation between the rate of BCAA disposal into proteins and oxidation across tissues (Figure 2J).

Finally, we estimated the tissue distribution of BCAA disposal at the whole-body level, by combining our calculated tissue BCAA oxidation flux and rates of BCAA disposal into protein synthesis with the total mass of each organ (Figure 2E and Table S2). This quantitative analysis indicates that the largest contributor to whole-body BCAA oxidation is the skeletal muscle (Figure 2K), while the largest contributors to BCAA disposal into protein synthesis are the liver, pancreas, and the skeletal muscle (Figure 2L). Together, the cumulative oxidation and deposition into protein calculated in this fashion account for about 50% of the measured rate of disposal ($R_d$) in each experiment (Figure S2I). The remainder likely reflects oxidation and protein synthesis in tissues not collected. For example, skin, bone marrow, and gut could account for ~32% of mouse protein and all of these tissues likely have high protein turnover (Preedy et al., 1983).

## Transcriptional and metabolic regulation of BCAA oxidation.

Different pathophysiological conditions can affect the tissue distribution of BCAA oxidation. Endurance exercise, for example, promotes BCAA oxidation in skeletal muscle (Shimomura et al., 2004; Overmyer et al., 2015) although its effect on other tissues is unknown. Numerous transcriptional effects of endurance exercise in skeletal muscle are mediated by PPARg-coactivator-1alpha (PGC-1α) (Puigserver and Spiegelman, 2003; Chinsomboon et al., 2009). PGC-1α overexpression in skeletal muscle (MCKα transgenic mice) strongly induces gene expression of nearly all BCAA catabolic enzymes (Figure 3A; Hatazawa et al., 2014; Jang et al. 2016). This observation motivated us to quantify the effects of these transcriptional changes on systemic BCAA oxidation. Isotope tracing after an intravenous bolus of $^{13}$C-valine (with unlabeled other BCAAs) showed similar labeling of circulating valine metabolites in wild-type and MCKα mice (Figures 3B and 3C). On the other hand, we observed ~7 and ~15-fold increase in TCA labeling in tibialis anterior (TA)

and quadriceps (Quad) muscle, respectively, compared to controls (Figures 3D and S3A). TCA labeling in other tissues were relatively unchanged (Figures 3D and S3A). The total pool size of TCA intermediates was similar or only slightly higher in MCKα muscle (Figure S3B), indicating that the higher labeling in TCA is not due to pool size difference but due to higher BCAA oxidation into TCA cycle. The pool size of 3-HIB in MCKα plasma was elevated, and rose much more significantly in response to a bolus of valine, compared to control plasma (Figure S3C), consistent with muscle being a large contributor to circulating plasma 3-HIB. Thus, transcriptional induction of BCAA catabolic genes in skeletal muscle, an adaptive response process that occurs in endurance-exercise training, dramatically increased muscle capacity for BCAA oxidation.

BCAA metabolism is also regulated by BCKDK-mediated phosphorylation of the BCKDH E1α subunit, BCKDHA (Figure 4A). To assess BCKDK-dependent regulation of systemic BCAA oxidation kinetics, we turned to BCKDK knockout (KO) mice. Western blotting demonstrated dramatic reduction of BCKDHA phosphorylation in all the tissues that we examined (Figure S4A), confirming BCKDK as a dominant regulator of BCKDH phosphorylation in most tissues. We next gavaged the KO mice with $^{13}$C-isoleucine and unlabeled leucine and valine, and measured circulating metabolites over time. At baseline, circulating BCAAs in the KO mice were half that in control, and circulating BCKAs were five times lower (Figures 4B, 4C, S4B, and S4C), consistent with hyperactivation of BCKDH. After gavage, the clearance of circulating valine and concomitant production of circulating 3-HIB was markedly (2-fold) increased in the KO mice (Figures 4B and 4D). Circulating levels of labeled succinate from $^{13}$C-isoleucine were also doubled in the KO mice (Figure 4E), demonstrating enhanced systemic BCAA oxidation.

Intriguingly, we noticed that the αKIV-to-valine ratio was significantly reduced (2.5-fold) in the KO mice, and remained low throughout the time course (Figure 4F). This low ratio suggests that the KO mice have a limited source of nitrogen acceptors for transamination such as α-ketoglutarate and pyruvate (Brosnan and Brosnan, 2006). A new metabolic steady state was also observed in the persistent 7-fold higher 3-HIB to αKIV ratio in the KO mice (Figure 4G). Indeed, metabolomics of circulating metabolites showed decreased ratios of α-ketoglutarate to glutamate and pyruvate to alanine in the KO mice (Figures 4H and S4D), reflecting limited BCAA transamination that causes altered metabolic steady states in the absence of systemic BCKDK. Despite these remarkable reductions in circulating BCAAs and BCKAs levels, we found no difference in glucose clearance or circulating free fatty acids between the KO and control mice (Figures S4E and S4F). However, we did note reductions of some circulating acylglycerols in the KO mice (Figure S4G), suggesting a potential link between BCAA metabolism and lipid metabolism. Together, we conclude that BCKDK deficiency increases systemic BCAA oxidation and creates new metabolic steady states.

### Acute BCKDK inhibition activates BCAA oxidation specifically in skeletal muscle.

The above experiment evaluated the effects of life-long, genetic alterations in the regulation of BCAA oxidation. Therapeutic interventions, however, will likely entail acute pharmacological treatments. For example, phenylbutyrate, a compound already FDA-

approved for the treatment of urea cycle disorders, inhibits BCKDK and is currently in a clinical trial to lower circulating BCAAs in patients with maple-syrup-urine disease (NCT01529060, Brunetti-Pierri et al., 2011; Burrage et al., 2014). Thus, we next quantified the consequences of acute, pharmacological suppression of BCKDK, using the compound BT2, an inhibitor of BCKDK shown to prevent heart failure in rodents (Figure 5A) (Tso et al., 2014; Sun et al., 2016). We first infused mice with trace amounts of $^{13}$C-isoleucine (and unlabeled leucine and valine) to achieve steady state, and then quantified the response to a single intravenous injection of BT2 (Figure 5B). Circulating BT2 remained present for hours, indicating relatively slow clearance *in vivo* (Figure S5A). Within 30 minutes of the BT2 injection, circulating BCAAs and BCKAs dropped markedly, while 3-HIB steadily increased, indicating efficient stimulation of systemic BCAA oxidation (Figures 5C, 5D, and S5B-S5D). Interestingly, no change was observed in the labeling of circulating isoleucine after BT2 treatment, indicating that BT2-induced BCAA oxidation does not affect BCAA production from proteolysis (Figure 5E). Metabolomics revealed that BT2 affects BCAA metabolism most strongly but also showed a general decrease in circulating free fatty acids and a trend towards increase in acyl-carnitines (Figure S5E), suggesting altered fatty acid metabolism (White et al., 2018). Thus, acute systemic BCKDK inhibition increased BCAA oxidation and reduced circulating BCAAs, without affecting the endogenous release of isoleucine from protein stores.

We next investigated the tissues targeted by BT2. Interestingly, even though BT2 was detected in all tissues collected (Figure S5F), only the liver, skeletal muscle, and heart had significant decreases in BCKDHA phosphorylation (Figure 5F). Moreover, only skeletal muscle showed significantly increased isoleucine oxidation (Figure 5G). Together, these data demonstrate that acute BCKDK inhibition increases whole-body BCAA oxidation largely via skeletal muscle in healthy mice, and underscores the critical point that BCAA oxidation flux *in vivo* in specific tissues cannot be reliably predicted only by markers of enzymatic activity such as BCKDHA phosphorylation.

### Insulin increases the preference for BCAA oxidation in cardiac and skeletal muscle.

Given the well-established relationship of plasma BCAAs and insulin resistance, we next investigated the acute effects of insulin on tissue-specific BCAA oxidation, by employing hyperinsulinemic-euglycemic clamps. Insulin and glucose were infused to reach steady state, and once steady state was achieved, we superimposed an infusion of $^{13}$C-isoleucine plus unlabeled leucine and valine (Figure 6A). Circulating insulin rose three-fold during the clamp (Figure 6B), requiring high glucose infusions (Figure 6C) to maintain glucose at ~125 mg/dl (Figure 6D).

Relative to controls, insulin clamps significantly reduced circulating levels of BCAAs (Figure 6E and S6). Interestingly, insulin infusion had only a marginal effect on circulating isoleucine labeling (Figure 6F), indicating that endogenous isoleucine release from proteolysis was, if anything, mildly increased (Figure 6G). In contrast, insulin more than doubled the relative preference for isoleucine oxidation specifically in skeletal muscle and heart (Figure 6H). Thus, physiological levels of insulin increase the preference for BCAA oxidation selectively in striated muscle.

### Obese and diabetic mice redistribute whole-body BCAA oxidation

Lastly, we investigated whole-body BCAA oxidation in states of insulin resistance. To this end, we used two widely-studied models: high-fat-diet-induced obese mice (HFD), and leptin receptor-deficient obese mice (*db/db*). HFD mice typically consume slightly less food by weight than chow-fed mice, but the high lipid intake increases the net caloric intake and causes obesity (Rossmeisl et al., 2003). In contrast, *db/db* mice develop obesity from hyperphagia, combined with reduced metabolic activity of brown fat (Ramirez and Sprott, 1978). Both models develop insulin resistance (Figures S7E-S7F, S7J-S7K), but only the *db/db* model recapitulates elevations in plasma BCAAs observed in humans (Figures S7G and S7L) (Lynch and Adams, 2014).

*db/db* and littermate control mice differ dramatically in body weight (Figures 7A and S7A). We thus tested two different $^{13}$C-valine infusion rates: one adjusted for body-weight (effectively 2.0x higher dose in *db/db*) and another adjusted for the volume of systemic circulation (1.25x higher for *db/db*; Yen et al., 1970). The higher dose caused significantly higher labeling of valine in *db/db* circulation, while the lower dose resulted in similar valine labeling between WT and *db/db* (Figures 7B and S7B). In both cases, endogenous valine appearance and disposal were ~40% lower when normalized to body weight, while roughly equal in total (Figures 7C, S7C, S7D, and S7H), despite marked differences in body mass and food consumption. Thus, total BCAA disposal in *db/db* mice is not adequately increased to match increases in dietary BCAA intake.

The lower infusion rate (1.25x) achieved much more similar labeling fraction of circulating valine, αKIV, and 3-HIB between *db/db* and control (Figures 7B and S7I), and was thus used to examine BCAA oxidation in individual tissues. Strikingly, *db/db* mice profoundly alter their systemic apportion of BCAA oxidation: the contribution of valine carbons to succinate was decreased by ~60% and ~20% in white adipose tissues and liver, respectively, whereas relative contribution was increased by ~50% in skeletal muscle (Figure 7D). Together, these data demonstrate an overall blunted rate of BCAA oxidation in *db/db* mice (compared to increased food intake), and a marked shift in BCAA oxidation towards skeletal muscle.

We next turned our attention to the second model of insulin resistance, high-fat feeding, which shows relatively less obesity and insulin resistance than *db/db* mice. After 14 weeks of HFD, mice gained ~30% more body weight than control mice (Figure 7E). $^{13}$C isoleucine infusion, dosed according to body weight, resulted in ~20% labeling of plasma isoleucine in both HFD and control animals (Figure 7F). The endogenous isoleucine appearance and disposal were unchanged in HFD when normalize to body weight, while the total isoleucine disposal was increased by ~30% (Figures 7G and S7M). Thus, in contrast to *db/db* mice, total isoleucine disposal was increased in HFD mice roughly in proportion to body weight.

HFD led to 75% and 50% declines in TCA labeling from isoleucine in white and brown adipose tissues, respectively (Figure 7H). Oxidation of isoleucine in skeletal muscle tended to decline (Figure 7H), in sharp contrast to the strong increase seen in *db/db* mice (Figure 7D). Thus, as in *db/db* mice, HFD leads to substantial reductions in BCAA oxidation in

white adipose tissues, but the consequent repartition of BCAA oxidation among other tissues differs strikingly between HFD and *db/db* mice.

## DISCUSSION

Here we provide quantitative analysis of whole-body BCAA metabolism with *in vivo* isotope tracing of BCAAs and metabolomics. We used a combination of techniques, including bolus infusions, gastric gavage, and steady-state infusions. The bolus and gavage experiments revealed the rapid kinetics of BCAA metabolism *in vivo*, as well as the surprising ability of all tissues evaluated to oxidize BCAAs. Constant infusions allowed us to calculate, with minimal perturbation of the system: 1) the systemic rate of appearance of endogenous BCAAs from proteolysis; 2) the relative contribution of BCAA-derived carbons to TCA carbons in each tissue; and 3) the fractional contribution of BCAAs to protein synthesis in each tissue.

Our direct measurement of integrated BCAA oxidation in conscious animals differs from classical paradigms of indirect methods, which are largely based on *ex vivo* measurement of BCKDH activity in tissue lysates, or on relative changes in isotopic enrichment between affluent and effluent plasma across tissue beds (Goodwin et al., 1998; Suryawan et al., 1998; Herman et al., 2010; Tso et al., 2014; Shin et al., 2014). Our data, combined with organ weights and oxygen consumption as a proxy for TCA flux, allowed us to quantitatively model the distribution of whole-body BCAA oxidation. A number of assumptions limit the precision of our model, including the assumptions that protein synthesis occurs homogenously within a given organ, and that for many tissues oxygen consumption measured *ex vivo* approximates consumption *in vivo*. Nevertheless, the model generates an approximate holistic picture of systemic BCAA oxidation, revealing that muscle, brown fat, and liver, account for ~86% of measured whole-body BCAA oxidation, although brown fat may account for less oxidation at thermoneutrality. The contribution of brain, lung, and white fat is relatively small. The sum of modeled oxidation accounted for a similar fraction of the measured plasma turnover as did incorporation of BCAA into proteins, highlighting the quantitative significance of oxidation in BCAA homeostasis. Future evaluations under altered physiological conditions, such as thermoneutrality or active exercise, will be of interest.

The pancreas uses BCAA-derived carbons for a striking ~20% of its TCA cycle. This occurs most likely within the exocrine pancreas, which accounts for the majority of pancreatic mass (Schachter and Buteau, 2014) and which has higher expression of BCAT and BCKDH than the endocrine pancreas (Sweatt et al., 2004). Why the pancreas prefers BCAAs is unclear. Perhaps the exocrine pancreas consumes BCAAs and other amino acids, e.g., glutamine (Hui et al., 2017), rather than glucose to avoid interfering with glucose sensing in the adjacent islets. Alternatively, high BCAA oxidation may reflect high protein turnover, as we also measured the highest protein synthesis rates in pancreas, although overall we noted no correlation (either positive or negative) between rates of BCAA oxidation and protein synthesis among different tissues. Notably, patients with pancreatic ductal adenocarcinoma (PDAC) reveal increased circulating BCAA levels that precede other clinical manifestations (Mayers et al., 2014). These elevations may reflect reduced BCAA oxidation in more

glycolytic pancreatic tumors (Mayers et al., 2016) and increased adipose tissue wasting (Danai et al., 2018). Further evaluations of pancreatic BCAA oxidation, using exocrine pancreas-specific KO mice, will likely be of interest.

The flux-controlling step of BCAA oxidation is governed by BCKDK-mediated BCKDHA phosphorylation. We show that chronic genetic BCKDK deficiency profoundly increases systemic BCAA oxidation. Moreover, BCKDK KO mice maintained new metabolic steady states with altered ratios of αKIV to valine and 3-HIB to αKIV. It is likely that flux through BCKDH is limited by the upstream transamination reaction, as suggested by markedly altered α-ketoglutarate/glutamate and pyruvate/alanine ratios. It will be interesting to investigate the effect of nitrogen homeostasis on BCAA metabolism and vice versa, and to extend these studies with tissue-specific models. Acute inhibition of BCKDK by BT2 also revealed a dramatic induction of systemic BCAA oxidation, without affecting the rate of endogenous BCAA release from protein stores. A recent report showed that in diabetic rats, where BCKDK levels are highly elevated in the liver (She et al., 2007), BT2 increases hepatic BCKDH activity (White et al., 2018). In contrast, in healthy mice, where liver BCKDH is mostly unphosphorylated (Joshi et al., 2006), BT2 activates BCAA oxidation primarily in skeletal muscle, despite suppressing the phosphorylation of BCKDH in other organs including the liver and heart. Thus, tissue BCAA oxidation flux cannot be predicted only by BCKDH phosphorylation, and is likely dictated by numerous other factors, including: the concentration of each enzyme substrate, which may be differentially affected by for example transport mechanisms; other post-translational and allosteric regulation of BCKDH; variable product-inhibition by for example NADH, acyl-CoAs; or altered relative contribution to the TCA cycle of other competing fuel (e.g., glycolysis, fatty acid beta-oxidation, or glutaminolysis). These observations underscore the critical point that BCAA metabolic flux *in vivo* cannot reliably be predicted by BCKDHA phosphorylation status alone (nor levels of mRNA expression or protein content), and instead requires integrated measurements in the intact organism, as we perform here.

Insulin potently suppresses protein catabolism (Castellino et al., 1987; Heslin et al., 1992). Surprisingly, we did not find large changes in endogenous BCAA release upon insulin treatment. Instead, insulin acutely increased BCAA oxidation in the heart and skeletal muscle. Why does insulin increase BCAA oxidation in these tissues? One possibility is that insulin powerfully inhibits lipolysis in white adipose tissue, thereby suppressing mobilization of fatty acids for consumption by other organs. The heart and skeletal muscle are especially avid consumers of circulating fatty acids. Thus, faced with reduced supply of fatty acids, these organs likely maintain TCA flux by increasing oxidation of, among other substrates, BCAAs. Insulin-driven changes in adipose fatty acid metabolism may hence indirectly control BCAA metabolism in striated muscle, much as they have recently been appreciated to indirectly control hepatic glucose output (Perry et al., 2015; Titchenell et al., 2016).

Human epidemiological and genetic data unequivocally associate elevations in BCAAs with insulin resistance and diabetes (Felig et al., 1969; Newgard et al., 2009; Wang et al., 2011; Lotta et al., 2016). Genetic animal models of insulin resistance (including *db/db* and *ob/ob* mice, Zucker fatty rats, and others) recapitulate these elevations in circulating BCAAs

(Lynch and Adams, 2014). Here we show that *db/db* mice have a dramatically altered distribution of whole-body BCAA oxidation, shifting oxidation away from white adipose and liver and towards skeletal muscle. The suppression of oxidation in fat and liver is consistent with the reported reduced expression of BCATs and BCKDH subunits in fat, and increased BCKDK expression in liver, of obese subjects, respectively (She et al., 2007; Lackey et al., 2013). Why is BCAA oxidation increased in muscle? The most likely explanation is that reduced BCAA oxidation in white fat and liver induces BCAA overflow to skeletal muscle, driving its BCAA oxidation there. As demonstrated in the BT2 experiments, skeletal muscle has a high capacity for increased BCAA oxidation, and therefore becomes the metabolic sink for defective BCAA oxidation in other organs (White et al., 2016). Thus, the total BCAA oxidation flux is maintained in *db/db* mice, but the systemic partitioning of BCAA oxidation is dramatically shifted (Figure 7I).

Several groups have proposed mechanisms connecting excess BCAA oxidation flux in skeletal muscle to the development of lipotoxicity and insulin resistance. One model proposes that excess BCAA oxidation competes for lipid oxidation, thus causing accumulation of toxic lipid intermediates (White et al., 2016). We find, however, that the fractional contribution of BCAA to the TCA in skeletal muscle is much smaller (5-6%) than that of fatty acids (40%, unpublished data), so that even a 50% increase in BCAA oxidation is not likely to significantly compete with fatty acids. Alternatively, excess BCAA oxidation may drive accumulation of acyl-carnitines by other means, including depletion of glycine and reduced acyl-glycine export (White et al., 2016). Additionally, elevated BCAA oxidation in skeletal muscle could drive increased secretion of 3- HIB, which promotes fatty acid transport across the endothelial barrier and subsequent lipotoxicity and insulin resistance (Jang et al., 2016). Each of these processes are likely aggravated by the simultaneous higher levels of circulating fatty acids elicited by insulin resistance in adipose tissue. Thus, a vicious positive feedback may be set in motion, whereby insulin resistance promotes BCAA catabolism in muscle, which in turn worsens insulin resistance (Figure 7I). If true, this model provides numerous opportunities for novel therapeutic targets.

Compared to *db/db* mice, HFD mice also suppress BCAA oxidation in adipose tissues, but BCAA oxidation is not shifted to skeletal muscle. Thus, the redistribution of BCAA oxidation in *db/db* and HFD mice differ markedly, underscoring the differing pathophysiological processes occurring in these two models. *db/db* mice are markedly hyperphagic, and BCAA oxidation is insufficient to compensate for the increased dietary absorption of BCAAs. In contrast, mice fed a HFD do not consume more BCAAs than chow-fed controls, achieving obesity via fat-based caloric intake instead. Thus, while excess BCAA consumption and oxidation likely contribute to the development of insulin resistance in *db/db* mice, the same mechanism may be less critical for HFD, although it is important to note that low BCAA diets also do protect against insulin resistance in HFD models (White et al., 2016, Maida et al., 2016; Cummings et al., 2018). These differences underscore the need for comprehensive and integrated studies, such as this one, in order to understand whole-body metabolic fate of metabolites in health and diseases.

### Limitations of study

Our work, though comprehensive, was limited to the evaluation of mice, and extrapolation to humans must therefore be done with care. We limited our steady-state infusions to as low amounts of added BCAAs as possible while still being able, technically, to detect $^{13}C$ enrichment in various tissues. Nevertheless, the system was not fully unperturbed by our infusions, as demonstrated by the mild rises in plasma BCAAs during prolonged infusions. Experiments with much lower infusion rates might become possible in the future as mass spectrometry technology and analytical methods improve enough to reliably quantitate very low labeling of downstream metabolites with large pools in tissues. Some experiments may not have reached a perfect steady state, but extremely long infusions would be confounded by changes in the physiological state of the mouse and technical complications from significant labeling in protein, and the slight changes observed do not significantly affect our interpretation of the results.

## STAR METHODS

### CONTACT FOR REAGENT AND RESOURCE SHARING

Requests for resources and/or further information should be directed to Dr. Zoltan P. Arany (zarany@pennmedicine.upenn.edu).

### EXPERIMENTAL MODEL AND SUBJECT DETAILS

**Administration of BCAAs to mice—**Animal studies followed protocols approved by the University of Pennsylvania, Princeton University, and Rutgers, University Institutional Animal Care and Use Committee. The mice were on normal light cycle (8 AM – 8 PM). *In vivo* infusion was performed on 10-14 week old male C57BL/6 mice or *db/db* mice with a catheter surgically implanted on the right jugular vein. Infusion was performed for 2~4 h to achieve isotopic steady state. The mouse infusion setup (Instech Laboratories, Plymouth Meeting, PA) included a tether and swivel system so that the animal has free movement in the cage with betting materials and free access to food and water. A mixture of BCAAs, one labeled with [U-$^{13}C$] (Cambridge Isotope Laboratories, Tewksbury, MA) with unlabeled other two BCAAs was prepared as solutions in normal saline and infused via the catheter at a constant rate (0.0836 μl/g/min). Doses were selected to minimize perturbation of BCAA homeostasis and are reported in Table S3. Infusions and injections began at 12 PM. For the oral gavage experiment, 14 week old male wild-type and BCKDK whole-body knockout mice were used (Joshi et al., 2006). On the day of the experiment, mice were transferred to new cages without food at 10 AM for fasting. At 3 PM, mice were gavaged a 1:1:1 mixture of [U-$^{13}C$]-isoleucine and unlabeled leucine and valine (30 mg/kg body weight, 10 μl/g body weight) in normal saline (46 mM each in 0.9% NaCl in water) via a plastic feeding tube (Instech Laboratories, Plymouth Meeting, PA). For the hyperinsulinemic-euglycemic clamp, insulin was infused at 2.5 mU/kg/min at 3.3 μl/min, and fasted controls were infused with saline at 6 μl/min to match the insulin + glucose infusion rate in clamped mice. For the BT2 experiment, BT2 (Sigma 592862) was dissolved in saline and injected (40 mg/kg). Blood samples (~20 μl) were collected by tail bleeding in lithium-heparin coated tubes (Sarstedt 16.443.100) and placed on ice for 20 min, and centrifuged at 16,000 x g for 10 min at 4°C. For tissue harvest, mice were euthanized with cervical dislocation or pentobarbital injection

and tissues were quickly dissected and snap frozen in liquid nitrogen with a pre-cooled Wollenberger clamp (Wollenberger et al., 1960). For the kinetic experiment (Figure 1), three sets of mice were each given a bolus of all three BCAAs (with one of BCAAs $^{13}$C-labeled). Plasma was collected between 0.5 and 1.5 minutes (indicated as 1 minute), between 2.5 and 3.5 minutes (indicated as 3 minutes) and 4.0 and 5.0 minutes (indicated as 5 minutes). Each set of animals was then sacrificed at the indicated time point by cervical dislocation, and the indicated tissues were immediately harvested and snap-frozen by a team of well-trained scientists within 1.5 minutes of cervical dislocation in the following order: heart + quad, liver, pancreas, gWAT, and BAT. Serum and tissue samples were kept at −80° until LC-MS a nalysis. All experiments were performed with 3-4 mice per day and data were combined from multiple litters / cages and repeated experiments from different days.

## METHOD DETAILS

### Metabolite measurement

To extract metabolites from serum samples, 100 μl −20° 40:40:20 methanol:acetonitrile:water (extraction solvent) was added to 5 μl of serum sample and incubated in −20°C for 1 hour, followed by vortexing and centrifugation at 16,000 x g for 10 min at 4°C. The supernatant (first extract) was transferred to a new tube. Then, 50 μl extraction solution was added to resuspend the pellet, followed by vortexing and centrifugation at 16,000 x g for 10 min at 4°C. The supernatant (second extract) was combined with the first extract. Then, 3 μl among the 150 μl extract was loaded to LC-MS. To extract metabolites from tissue samples, frozen tissue samples were ground at liquid nitrogen temperature with a Cryomill (Retsch, Newtown, PA). The resulting tissue powder (~20 mg) was weighed. The extraction was then done by adding −20°C extraction solvent to the powder and incubated in −20°C for an hour, followed by vortexing and centrifugation at 16,000 x g for 10 min at 4°C. The volume of the extraction solution (μl) was 40 x the weight of tissue (mg) to make an extract of 25 mg tissue per ml solvent. Serum and tissue extracts were analyzed by LC-MS. A quadrupole-orbitrap mass spectrometer (Q Exactive, Thermo Fisher Scientific, San Jose, CA) operating in negative or positive ion mode was coupled to hydrophilic interaction chromatography via electrospray ionization and used to scan from m/z 70 to 1000 at 1 Hz and 75,000 resolution. LC separation was on a XBridge BEH Amide column (2.1 mm × 150 mm, 2.5 μm particle size, 130 Å pore size; Waters, Milford, MA) using a gradient of solvent A (20 mM ammonium acetate, 20 mM ammonium hydroxide in 95:5 water: acetonitrile, pH 9.45) and solvent B (acetonitrile). Data were analyzed using the MAVEN software (Melamud et al., 2010). Isotope labeling was corrected for natural $^{13}$C abundance (Su et al., 2017). Flow rate was 150 μl/min. The LC gradient was: 0 min, 85% B; 2 min, 85% B; 3 min, 80% B; 5 min, 80% B; 6 min, 75% B; 7 min, 75% B; 8 min, 70% B; 9 min, 70% B; 10 min, 50% B; 12 min, 50% B; 13 min, 25% B; 16 min, 25% B; 18 min, 0% B; 23 min, 0% B; 24 min, 85% B; 30 min, 85% B. Autosampler temperature is 5 °C, and injection volume is 3 μL.

### Lipid measurement

Serum samples (10 μL) was dissolved in 0.5 mL of 0.1 M HCl/methanol (50/50). Then, 0.25 mL of chloroform was added and vortexed for 10 seconds. After centrifugation at 14,000 g

at 4°C for 10 min, bottom layer was collected with a glass syringe and transferred to a glass MS vial. Samples were then dried under a stream of N2, dissolved in 100 μL of isopropanol:methanol (1:1, v/v) solution and injected into a 1290 Infinity UHPLC system coupled to Agilent 6550 iFunnel Q-TOF mass spectrometer. To cover both the positive charged and negative charged species, each sample was analyzed twice using the same LC gradient but with different mass spectrometer ionization modes. The LC separation was performed on an Agilent Poroshell 120 EC-C18 column (150 × 2.1 mm, 2.7 μm particle size) with a flow rate of 150 μL/min. Solvent A was 1 mM ammonium acetate + 0.2% acetic acid in water/methanol (90:10). Solvent B was 1 mM ammonium acetate + 0.2% acetic acid in methanol/2-propanol (2:98). The solvent gradient in volume ratios was as follows: 0-2 min, 25% B; 2-4 min, 25 to 65% B; 4-16 min, 65 to 100% B; 16-20 min, 100% B; 20-21 min, 100 to 25% B; 21-27 min, 25% B. Data obtained by QTOF were first converted into mzXML format and then processed using MAVEN software to obtain the signal intensity of ~200 lipid species.

### Western Blots

Tissues were lysed by RIPA buffer containing phosphatase and proteinase inhibitors (PhosSTOP and Complete miniproteinase inhibitor cocktail, Roche). Pancreas samples were lysed in RIPA with the following protease inhibitors: 0.1 mM AEBSF HCl, 0.08 μM Aprotinin, 5 μM Bestatin, 1.5 μM E-64, 2 μM Leupeptin Hemisulfate and 1 μM Pepstatin and the following phosphatase inhibitors: 1 mM NaF and 1 mM $Na_3VO_4$. Protein concentration was quantified by BCA protein assay kit (Thermo Fisher Scientific), and the same amount of protein (10–20 μg) was loaded to 4%–20% gradient Tris-glycine polyacrylamide gel (Bio-Rad) and electrophoresed (SDS-PAGE). After the SDS-PAGE, protein samples were transferred to PVDF membrane (Millipore). Membranes were blocked by 5% skim milk for 1 h and then incubated with the respective primary antibodies: BCKDK (Sigma, HPA017995), phospho-BCKDHA S293 (Bethyl, A304-672A), and total BCKDHA (Bethyl A303-790A). Appropriate HRP-conjugated secondary antibodies were selected according to the host species of primary antibodies, and images were taken by using a digital imager (GE Healthcare Life Sciences, ImageQuant LAS 4000). The result was quantified using ImageJ.

## QUANTIFICATION AND STATISTICAL ANALYSIS

### Quantification of protein fractional synthesis rate (FSR) and whole-body BCAA disposal to proteins

Tissue protein samples from the $^{13}$C-leucine infusion were used to quantify FSR (Rennie et al., 1982). Briefly, labeling of leucine in the proteins was normalized to plasma leucine labeling. Because the $^{13}$C-leucine infusion used to measure protein labeling was not primed, labeling in the precursor pool was not at an instantaneous steady state. To account for the labeling kinetics during the infusion, we calculated the precursor labeling ($A_p$) as the area-under-the-curve of the first-order non-linear best fit equation for plasma leucine labeling for each mouse (Graphpad). The labeling in protein-derived leucine was then normalized to $A_p$ to calculate FSR. Calculated FSR was then used to model whole-body BCAA disposal, by

incorporating the total amount of protein in each tissue, and the known molar ratio of BCAA content in animal protein, to calculate the rate of BCAA disposal into protein.

$$\frac{fraction\ synthesized}{minute} * \frac{g\ protein}{g\ tissue} * \frac{mol\ BCCA}{g\ protein} = \frac{mol\ BCAA}{minute * g\ tissue}$$

This rate of protein synthesis is multiplied by the total organ weight (for a 25g mouse) to model BCAA disposal into protein in the entire organ.

$$\frac{mol\ BCAA}{minute * g\ tissue} * \frac{g\ tissue}{organ} = \frac{mol\ BCAA}{minute * organ}$$

This model makes several assumptions. First, we assume the protein content and FSR of a given tissue is the same for the entire organ. Second, we represent the protein in a given tissue as a single well-mixed pool. Although these assumptions have some limitations, they allow for reasonable estimates of total protein turnover at the whole-body levels.

## Quantification of whole-body oxidation flux

For a given tissue, this model utilizes the measured fractional contribution of one BCAA to TCA cycle intermediates (average of succinate and malate), and then multiplies this fraction by the modeled TCA cycle turnover. This generates flux of BCAA oxidation per gram tissue, which is then multiplied by the total mass of that tissue in the mouse to generate the BCAA oxidation flux for the entire organ. Total TCA turnover from all sources (as moles reducing equivalents produced per minute) is derived from $VO_2$, based on the principle that production of reducing equivalents is mostly coupled to oxygen consumption at steady state (Randle et al., 1970; Malloy et al., 1996).

$$\frac{mol\ Reducing\ Equivalents}{minute * g} = 2 * \frac{mol\ O_2}{minute * g}$$

The TCA cycle produces ~2/3 of the reducing equivalents derived from the major TCA cycle substrates (glucose, lactate, fat, etc). Therefore, the production of reducing equivalents in the TCA cycle is approximately 2/3 of total production.

$$\frac{mol\ Red.\ Equiv.\ from\ TCA}{minute * g} = \frac{2}{3} * 2 * \frac{mol\ O_2}{minute * g}$$

Applying the measured fraction of TCA derived from a BCAA gives the flux of reducing equivalents produced inside the TCA cycle by that BCAA.

$$\frac{mol\ Red.\ Equiv.\ from\ TCA}{minute * g} * \frac{BCAA}{TCA} = \frac{mol\ Red.\ Equiv.\ made\ in\ TCA\ from\ BCAA\ carbons}{minute * g}$$

Each BCAA supplies a specific number of reducing equivalents via the TCA (valine supplies 6, leucine and isoleucine supply 10). This constant can be used to convert reducing equivalents to BCAAs entering TCA.

$$\frac{mol\ Red\ .\ Equiv\ .\ made\ in\ TCA\ from\ BCAA\ carbons}{minute * g} * \frac{mol\ BCAA}{mol\ Red\ .\ Equiv\ .\ made\ in\ TCA} = \frac{mol\ BCCA}{minute * g}$$

This flux of oxidation per gram of tissue was multiplied by the total organ mass to determine the whole-organ oxidation flux (as in the model of whole-body disposal into protein). Values for $VO_2$ and whole-organ mass were sourced from published material as indicated in Table S1 (Martin and Furhman, 1955; Abreu-Vieira et al., 2015; Boudina et al., 2005; Lenzen, 1979; Schefer and Talan, 1996; Desai et al., 1997, Trayhurn and James, 1978).

### Statistics

A two-tailed unpaired Student's t-test was used to calculate p-value. For experiments with multiple comparisons (i.e. tissue labeling), Student's t-test followed by correction for a false discovery rate (FDR) of 0.05 was used to calculate q-values. For plasma experiments with repeated measurements, two-way ANOVA followed by correction for a FDR of 0.05 was used to calculate q-values. For metabolomics, Student's t-test followed by correction for an FDR of 0.05 was used to calculate q-values. Data are displayed as mean ± SE. Animals were randomized to treatment groups. Infusion experiments were performed in 3-4 mice per day, requiring multiple litters and cohorts. All measurements were performed blinded to treatment or genotype.

## DATA AND SOFTWARE AVAILABILITY

For all infusion experiments, the relative totals (ion counts), raw $^{13}C$-labeling (% carbons), and Normalized Labeling (% carbons normalized to labeling in the tracee from plasma collected at the end of the infusion) of relevant metabolites (including lactate, glucose, and glutamine) are available in Table S1.

## Supplementary Material

Refer to Web version on PubMed Central for supplementary material.

## ACKNOWLEDGEMENTS

C.J. is a postdoctoral fellow of the American Diabetes Association (1-17-PDF-076). S.H. is a Merck Fellow of the Life Sciences Research Foundation. This work was supported by grants from the National Institutes of Health (T32-GM07229 to M.D.N., DK109714 to T.G.A., and HL094499 and DK107667 to Z.A.), support from the DRC Regional Metabolomics Core (P30 DK19525), and an Established Investigator Award from the American Heart Association (Z.A.). We thank Emily Mirek in the Anthony lab for technical support, and members of the Arany lab and the Rabinowitz lab, Mitchel Lazar, William Quinn and Joseph Baur for scientific discussions.

## REFERENCES

Abreu-Vieira G, Xiao C, Gavirlova O, Retiman ML (2015). Integration of body temperature into the analysis of energy expenditure in the mouse. Mol Met. 4, 461–470.

Anthony JC, Yoshizawa F, Anthony TG, Vary TC, Jefferson LS, and Kimball SR (2000). Leucine stimulates translation initiation in skeletal muscle of postabsorptive rats via a rapamycin-sensitive pathway. J. Nutr 130, 2413–2419. [PubMed: 11015466]

Bachmanov AA, Reed DR, Beauchamp GK, and Tordoff MG (2002). Food intake, water intake, and drinking spout side preference of 28 mouse strains. Behav. Genet 32, 435–443. [PubMed: 12467341]

Boudina S, Sena S, O'Neill BT, Tathireddy P, Young ME, and Abel ED (2005). Reduced mitochondrial oxidative capacity and increased mitochondrial uncoupling impair myocardial energetics in obesity. Circulation 112, 2686–2695. [PubMed: 16246967]

Burrage LC, Jain M, Gandolfo L, Lee BH, Members of the Urea Cycle Disorders Consortium, and Nagamani SC (2014). Sodium phenylbutyrate decreases plasma branched-chain amino acids in patients with urea cycle disorders. Mol. Genet. Metab 113, 131–135. [PubMed: 25042691]

Brosnan JT, and Brosnan ME (2006). Branched-chain amino acids: enzyme and substrate regulation. J. Nutr 136, 207S–211S. [PubMed: 16365084]

Brunetti-Pierri N, Lanpher B, Erez A, Ananieva EA, Islam M, Marini JC, Sun Q, Yu C, Hegde M, Li J, et al. (2011). Phenylbutyrate therapy for maple syrup urine disease. Hum. Mol. Genet 20, 631–640. [PubMed: 21098507]

Castellino P, Luzi L, Simonson DC, Haymond M, and DeFronzo RA (1987). Effect of insulin and plasma amino acid concentrations on leucine metabolism in man. Role of substrate availability on estimates of whole body protein synthesis. J. Clin. Invest 80, 1784–1793. [PubMed: 3316280]

Chinsomboon J, Ruas J, Gupta RK, Thom R, Shoag J, Rowe GC, Sawada N, Raghuram S, Arany Z (2009). The transcriptional coactivator PGC-1alpha mediates exercise-induced angiogenesis in skeletal muscle. Proc. Natl. Acad. Sci. USA 106, 21401–21406. [PubMed: 19966219]

Cummings NE, Williams EM, Kasza I, Konon EN, Schaid MD, Schmidt BA, Poudel C, Sherman DS, Yu D, Arriola Apelo SI, et al. (2018). Restoration of metabolic health by decreased consumption of branched-chain amino acids. J. Physiol 596, 623–645. [PubMed: 29266268]

Danai LV, Babic A, Rosenthal MH, Dennstedt EA, Muir A, Lien EC, Mayers JR, Tai K, Lau AN, Jones-Sali P, et al. (2018). Altered exocrine function can drive adipose wasting in early pancreatic cancer. Nature 558, 600–604. [PubMed: 29925948]

Davis TA, Nguyen HV, Garcia-Bravo R, Fiorotto ML, Jackson EM, Lewis DS, Lee DR, and Reeds PJ (1994). Amino acid composition of human milk is not unique. J. Nutr 124, 1126–1132. [PubMed: 8027865]

Desai LH, Sato R, Schauble E, Barsh GS, Kobilka BK, Berstein D (1997). Cardiovascular indexes in the mouse at rest and with exercise: new tools to study models of cardiac disease. Am. J. Physiol. Heart Circ. Physiol 272, H1053–H1061.

Ding C, Li Y, Guo F, Jiang Y, Ying W, Li D, Yang D, Xia X, Liu. W, Zhao Y, et al. (2016). A cell-type-resolved liver proteome. Mol. Cell Proteomics 10, 3190–3202.

Felig P, Marliss E, and Cahill GF, Jr. (1969). Plasma amino acid levels and insulin secretion in obesity. N. Engl. J. Med 281, 811–816. [PubMed: 5809519]

Goodwin GW, Zhang B, Paxton R, and Harris RA (1998). Determination of activity and activity state of branched-chain alpha-keto acid dehydrogenase in rat tissues. Methods Enzymol. 166, 189–201.

Harper AE, Miller RH, and Block KP (1984). Branched-chain amino acid metabolism. Annu. Rev. Nutr 4, 409–454. [PubMed: 6380539]

Hatazawa Y, Tadaishi M, Nagaike Y, Morita A, Ogawa Y, Ezaki O, Takai-Igarashi T, Kitaura Y, Shimomura Y, Kamei Y, et al. (2014). PGC-1α-mediated branched-chain amino acid metabolism in the skeletal muscle. PLoS One 9, e91006. [PubMed: 24638054]

Herman MA, She P, Peroni OD, Lynch CJ, and Kahn BB (2010). Adipose tissue branched chain amino acid (BCAA) metabolism modulates circulating BCAA levels. J. Biol. Chem 285, 11348–11356. [PubMed: 20093359]

Heslin MJ, Newman E, Wolf RF, Pisters PW, and Brennan MF (1992). Effect of hyperinsulinemia on whole body and skeletal muscle leucine carbon kinetics in humans. Am. J. Physiol 262, E911–918. [PubMed: 1319683]

Huang Y, Zhou M, Sun H, and Wang Y (2011). Branched-chain amino acid metabolism in heart disease: an epiphenomenon or a real culprit? Cardiovasc. Res 90, 220–223. [PubMed: 21502372]

Hui S, Ghergurovich JM, Morscher RJ, Jang C, Teng X, Lu W, Esparza LA, Reya T, Le Zhan, Yanxiang Guo, J., et al. (2017). Glucose feeds the TCA cycle via circulating lactate. Nature 551, 115–118. [PubMed: 29045397]

Hutson SM, Wallin R, and Hall TR (1992). Identification of mitochondrial branched chain aminotransferase and its isoforms in rat tissues. J. Biol. Chem 267, 15681–15686. [PubMed: 1639805]

James HA, O'Neill BT, and Nair KS (2017). Insulin regulation of proteostasis and clinical implications. Cell Metab. 26, 310–313. [PubMed: 28712655]

Jang C, Oh SF, Wada S, Rowe GC, Liu L, Chan MC, Rhee J, Hoshino A, Kim B, Ibrahim A, et al. (2016). A branched-chain amino acid metabolite drives vascular fatty acid transport and causes insulin resistance. Nat. Med 22, 421–426. [PubMed: 26950361]

Jeyaraj D, Scheer FA, Ripperger JA, Haldar SM, Lu Y, Prosdocimo DA, Eapen SJ, Eapen BL, Cui Y, Mahabeleshwar GH, et al. (2012). Klf15 orchestrates circadian nitrogen homeostasis. Cell Metab. 15, 311–323. [PubMed: 22405069]

Joshi MA, Jeoung NH, Obayashi M, Hattab EM, Brocken EG, Liechty EA, Kubek MJ, Vattem KM, Wek RC, and Harris RA (2006). Impaired growth and neurological abnormalities in branched-chain alpha-keto acid dehydrogenase kinase-deficient mice. Biochem. J 400, 153–162. [PubMed: 16875466]

Lackey DE, Lynch CJ, Olson KC, Mostaedi R, Ali M, Smith WH, Karpe F, Humphreys S, Bedinger DH, Dunn TN, et al. (2013). Regulation of adipose branched-chain amino acid catabolism enzyme expression and cross-adipose amino acid flux in human obesity. Am. J. Physiol. Endocrinol. Metab 304, E1175–1187. [PubMed: 23512805]

Lau KS, Fatania HR, and Randle PJ (1982). Regulation of the branched chain 2-oxoacid dehydrogenase kinase reaction. FEBS Lett. 144, 57–62. [PubMed: 6980796]

Lenzen S (1979). Insulin secretion by isolated perfused rat and mouse pancreas. Am. J. Physiol 236, E391–400. [PubMed: 373466]

Lotta LA, Scott RA, Sharp SJ, Burgess S, Luan J, Tillin T, Schmidt AF, Imamura F, Stewart ID, Perry JR, et al. (2016). Genetic predisposition to an impaired metabolism of the branched-chain amino acids and risk of type 2 diabetes: A mendelian randomisation analysis. PLoS Med. 13, e1002179. [PubMed: 27898682]

Lu G, Sun H, She P, Youn JY, Warburton S, Ping P, Vondriska TM, Cai H, Lynch CJ, and Wang Y (2009). Protein phosphatase 2Cm is a critical regulator of branched-chain amino acid catabolism in mice and cultured cells. J. Clin. Invest 119, 1678–1687. [PubMed: 19411760]

Lynch CJ, and Adams SH (2014). Branched-chain amino acids in metabolic signalling and insulin resistance. Nat. Rev. Endocrinol 10, 723–736. [PubMed: 25287287]

Mahendran Y, Jonsson A, Have CT, Allin KH, Witte DR, Jørgensen ME, Grarup N, Pedersen O, Kilpeläinen TO, and Hansen T (2017). Genetic evidence of a causal effect of insulin resistance on branched-chain amino acid levels. Diabetologia 60, 873–878. [PubMed: 28184960]

Maida A, Zota A, Sjøberg KA, Schumacher J, Sijmonsma TP, Pfenninger A, Christensen MM, Gantert T, Fuhrmeister J, Rothermel U, et al. (2016). A liver stress-endocrine nexus promotes metabolic integrity during dietary protein dilution. J. Clin. Invest 126, 3263–3278. [PubMed: 27548521]

Malloy CR, Jones JG, Jeffrey FM, Jessen ME, and Sherry AD (1996). Contribution of various substrates to total citric acid cycle flux and anaplerosis as determined by 13C isotopomer analysis and O2 consumption in the heart. MAGMA. 4, 35–46. [PubMed: 8774000]

Marcadier JL, Smith AM, Pohl D, Schwartzentruber J, Al-Dirbashi OY, FORGE Canada Consortium, Majewski J, Ferdinandusse S, Wanders RJ, Bulman DE, et al. (2013). Mutations in ALDH6A1 encoding methylmalonate semialdehyde dehydrogenase are associated with dysmyelination and transient methylmalonic aciduria. Orphanet. J. Rare Dis 8, 98. [PubMed: 23835272]

Martin AW, and Furhman FA (1955). The relationship between summated tissue respiration and metabolic rate in the mouse and dog. Physiol Zool. 28, 18–34.

Mayers JR, Wu C, Clish CB, Kraft P, Torrence ME, Fiske BP, Yuan C, Bao Y, Townsend MK, Tworoger SS et al. (2014). Elevation of circulating branched-chain amino acids is an early event in human pancreatic adenocarcinoma development. Nat. Med 20, 1193–1198. [PubMed: 25261994]

Mayers JR, Torrence ME, Danai LV, Papagiannakopoulos T, Davidson SM, Bauer MR, Lau AN, Ji BW, Dixit PD, Hosios AM, et al. (2016). Tissue of origin dictates branched-chain amino acid metabolism in mutant Kras-driven cancers. Science 353, 1161–1165. [PubMed: 27609895]

Melamud E, Vastag L, and Rabinowitz JD (2010). Metabolomic analysis and visualization engine for LC-MS data. Anal. Chem 82, 9818–9826. [PubMed: 21049934]

Newgard CB, An J, Bain JR, Muehlbauer MJ, Stevens RD, Lien LF, Haqq AM, Shah SH, Arlotto M, Slentz CA, et al. (2009). A branched-chain amino acid-related metabolic signature that differentiates obese and lean humans and contributes to insulin resistance. Cell Metab. 9, 311–326. [PubMed: 19356713]

Overmyer KA, Evans CR, Qi NR, Minogue CE, Carson JJ, Chermside-Scabbo CJ, Koch LG, Britton SL, Pagliarini DJ, Coon JJ, et al. (2015). Maximal oxidative capacity during exercise is associated with skeletal muscle fuel selection and dynamic changes in mitochondrial protein acetylation. Cell Metab. 21, 468–478. [PubMed: 25738461]

Perry RJ, Camporez JP, Kursawe R, Titchenell PM, Zhang D, Perry CJ, Jurczak MJ, Abudukadier A, Han MS, Zhang XM et al. (2015). Hepatic acetyl CoA links adipose tissue inflammation to hepatic insulin resistance and type 2 diabetes. Cell 160, 745–758. [PubMed: 25662011]

Preedy VR, McNurlan MA, and Garlick PJ (1983). Protein synthesis in skin and bone of the young rat. Br J Nutr. 49, 517–523. [PubMed: 6190506]

Puigserver P, and Spiegelman BM (2003). Peroxisome proliferator-activated receptorgamma coactivator 1 alpha (PGC-1 alpha): transcriptional coactivator and metabolic regulator. Endocr. Rev 24, 78–90. [PubMed: 12588810]

Randle PJ, England PJ, and Denton RM (1970). Control of the tricarboxylate cycle and its interactions with glycolysis during acetate utilization in rat heart. Biochem. J 117, 677–695. [PubMed: 5449122]

Ramirez I, and Sprott RL (1978). Food intake and body weight regulation in diabetes (db/db) and obese (ob/ob) mice. Physiological Psychology. 6, 187–190.

Rennie MJ, Edwards RHT, Halliday D, Matthews DE, Wolman SL, and Millward DJ (1982). Muscle protein synthesis measured by stable isotope techniques in man: the effects of feeding and fasting. Clin. Sci 63, 519–523. [PubMed: 6181926]

Roberts LD, Boström P, O'Sullivan JF, Schinzel RT, Lewis GD, Dejam A, Lee YK, Palma MJ, Calhoun S, Georgiadi A, et al. (2014). β-Aminoisobutyric acid induces browning of white fat and hepatic β-oxidation and is inversely correlated with cardiometabolic risk factors. Cell Metab. 19, 96–108. [PubMed: 24411942]

Rossmeisl M, Rim JS, Koza RA, and Kozak LP (2003). Variation in type 2 diabetes--related traits in mouse strains susceptible to diet-induced obesity. Diabetes 52, 1958–1966. [PubMed: 12882911]

Schachter D, and Buteau J (2014). Glutamate formation via the leucine-to-glutamate pathway of rat pancreas. Am. J. Physiol. Gastrointest. Liver Physiol 306, G938–946. [PubMed: 24699330]

Schefer V, and Talan MI (1996). Oxygen consumption in adult and AGED C57BL/6J mice during acute treadmill exercise of different intensity. Exp. Gerontol 31, 387–392. [PubMed: 9415121]

Shimomura Y, Murakami T, Nakai N, Nagasaki M, and Harris RA (2004). Exercise promotes BCAA catabolism: effects of BCAA supplementation on skeletal muscle during exercise. J. Nutr 134, 1583S–1587S. [PubMed: 15173434]

She P, Van Horn C, Reid T, Hutson SM, Cooney RN, and Lynch CJ (2007). Obesity-related elevations in plasma leucine are associated with alterations in enzymes involved in branched-chain amino acid metabolism. Am. J. Physiol. Endocrinol. Metab 293, E1552–1563. [PubMed: 17925455]

Shin AC, Fasshauer M, Filatova N, Grundell LA, Zielinski E, Zhou JY, Scherer T, Lindtner C, White PJ, Lapworth AL, et al. (2014). Brain insulin lowers circulating BCAA levels by inducing hepatic BCAA catabolism. Cell Metab. 20, 898–909. [PubMed: 25307860]

Su AI, Wiltshire T, Batalov S, Hilmar L, Ching KA, Block D, Zhang J, Soden R, Hayakawa M, and Kreiman G (2004). A gene atlas of the mouse and human proteinencoding transcriptomes. Proc. Natl. Acad. Sci. USA 101, 6062–6067. [PubMed: 15075390]

Su X, Lu W, and Rabinowitz JD (2017). Metabolite spectral accuracy on orbitraps. Anal. Chem 89, 5940–5948. [PubMed: 28471646]

Sun H, Olson KC, Gao C, Prosdocimo DA, Zhou M, Wang Z, Jeyaraj D, Youn JY, Ren S, Liu Y, et al. (2016). Catabolic defect of branched-chain amino acids promotes heart failure. Circulation 133, 2038–2049. [PubMed: 27059949]

Suryawan A, Hawes JW, Harris RA, Shimomura Y, Jenkins AE, and Hutson SM (1998). A molecular model of human branched-chain amino acid metabolism. Am. J. Clin. Nutr 68, 72–81. [PubMed: 9665099]

Sweatt AJ, Wood M, Suryawan A, Wallin R, Willingham MC, and Hutson SM (2004). Branched-chain amino acid catabolism: unique segregation of pathway enzymes in organ systems and peripheral nerves. Am. J. Physiol. Endocrinol. Metab 286, E64–76. [PubMed: 12965870]

Titchenell PM, Quinn WJ, Lu M, Chu Q, Lu W, Li C, Chen H, Monks BR, Chen J, Rabinowitz JD, et al. (2016). Direct hepatocyte insulin signaling is required for lipogenesis but is dispensable for the suppression of glucose production. Cell Metab. 23, 1154–1166. [PubMed: 27238637]

Trayhurn P, and James WPT (1978). Thermoregulation and non-shivering thermogenesis in the genetically obese (ob/ob) mouse. Pflugers Arch. 373, 189–193. [PubMed: 565045]

Tso SC, Gui WJ, Wu CY, Chuang JL, Qi X, Skvora KJ, Dork K, Wallace AL, Morlock LK, Lee BH, et al. (2014). Benzothiophene carboxylate derivatives as novel allosteric inhibitors of branched-chain α-ketoacid dehydrogenase kinase. J. Biol. Chem 289, 20583–20593. [PubMed: 24895126]

Wang Q, Holmes MV, Davey Smith G, and Ala-Korpela M (2017). Genetic support for a causal role of insulin resistance on circulating branched-chain amino acids and inflammation. Diabetes Care 40, 1779–1786. [PubMed: 29046328]

Wang TJ, Larson MG, Vasan RS, Cheng S, Rhee EP, McCabe E, Lewis GD, Fox CS, Jacques PF, Fernandez C, et al. (2011). Metabolite profiles and the risk of developing diabetes. Nat. Med 17, 448–453. [PubMed: 21423183]

White PJ, Lapworth AL, An J, Wang L, McGarrah RW, Stevens RD, Ilkayeva O, George T, Muehlbauer MJ, Bain JR, et al. (2016). Branched-chain amino acid restriction in Zucker-fatty rats improves muscle insulin sensitivity by enhancing efficiency of fatty acid oxidation and acyl-glycine export. Mol. Metab 5, 538–551. [PubMed: 27408778]

White PJ, McGarrah RW, Grimsrud PA, Tso SC, Yang WH, Haldeman JM, Grenier-Larouche T, An J, Lapworth AL, Astapova I, et al. (2018). The BCKDH Kinase and Phosphatase Integrate BCAA and Lipid Metabolism via Regulation of ATP-Citrate Lyase. Cell Metab. 27, 1281–1293. [PubMed: 29779826]

Wollenberger A, Ristau O, and Schoffa G (1960). Eine einfache Technik der extrem schnellen Abkühlung größerer Gewebestücke. Pflüger's Archiv für die gesamte Physiologie des Menschen und der Tiere 270, 399–412.

Wu C, Jin X, Tsueng G, Afrasiabi C, Su AI (2016). BioGPS: building your own mash-up of gene annotations and expression profiles. Nucleic Acids Res. 44, D313–D316. [PubMed: 26578587]

Yen TT, Stienmetz J, and Simpson PJ (1970). Blood volume of obese (ob-ob) and diabetic (db-db) mice. Proc. Soc. Exp. Biol. Med 133, 307–308. [PubMed: 5412353]

1. In vivo steady-state isotope tracing studies provide a quantitative framework of tissue BCAA oxidation.
2. Genetic and pharmacological perturbations alter whole-body tissue distribution of BCAA catabolism.
3. Insulin acutely increases BCAA oxidation selectively in striated muscle.
4. Insulin resistant mice mice shunt BCAA oxidation away from liver and fat, and toward skeletal muscle.

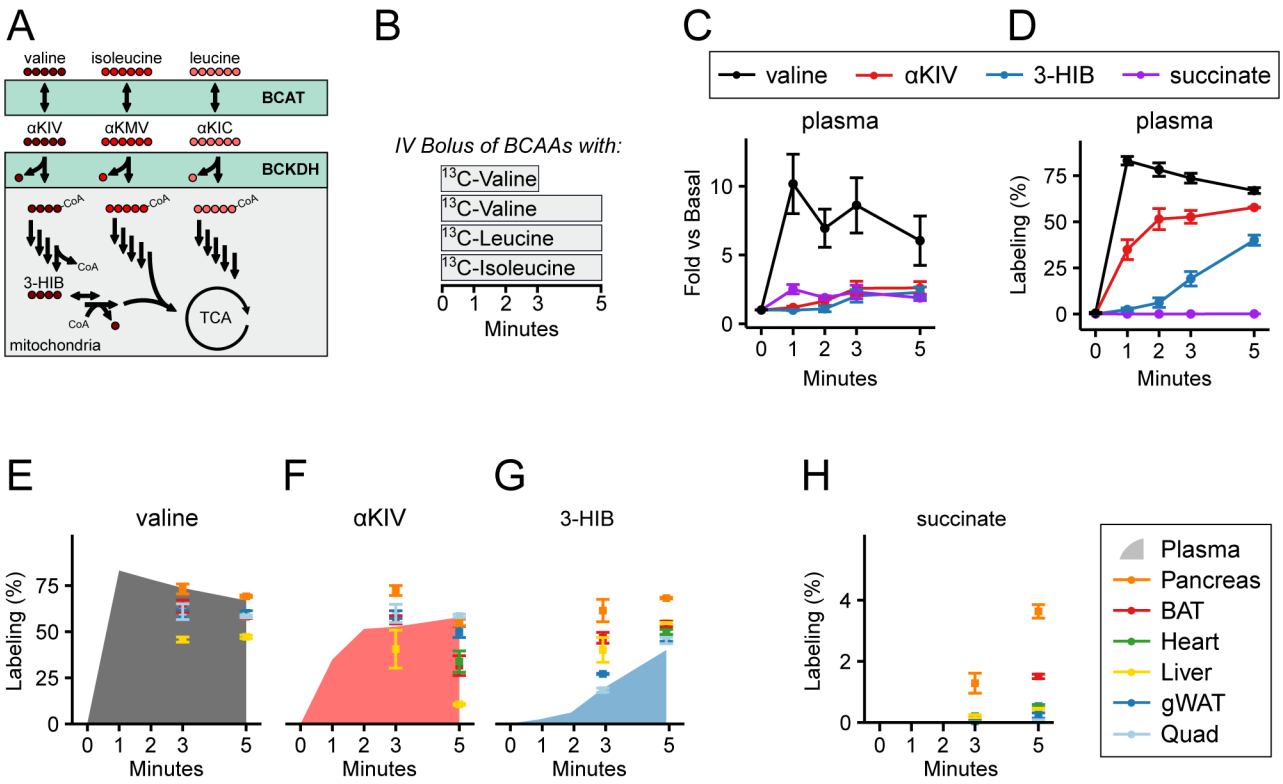


**Figure 1.** ***In vivo*** **isotopic tracing reveals rapid oxidation of BCAAs in multiple organs.**

(A) Schematic of BCAA oxidation pathway. BCAT transaminates BCAAs to BCKAs, which are subsequently oxidized by BCKDH. By this reaction, BCKAs lose one carbon as $CO_2$ and are conjugated to Co-enzyme A (CoA). All downstream intermediates are trapped in the mitochondria by CoA and oxidized into the TCA cycle, except for 3-HIB, which can be released to the circulation. (B) Experimental scheme. Mice received an intravenous bolus injection of BCAAs with one labeled with $^{13}C$ and the other two unlabeled. Blood was collected every 1 min, and tissues were harvested at 3 or 5 min. (C) Plasma levels of the indicated metabolites, normalized to time 0. (D) Valine oxidation is fast. Data show labeling (%) of the indicated metabolites in plasma. (E-H) Valine is oxidized by multiple organs. Data show labeling (%) of the indicated metabolites in plasma (shaded) and in the indicated tissues. N = 3-6. Data are means and error bars are ± SE. BAT and WAT, brown and white adipose tissue, respectively; Quad, quadriceps. See also Figure S1.

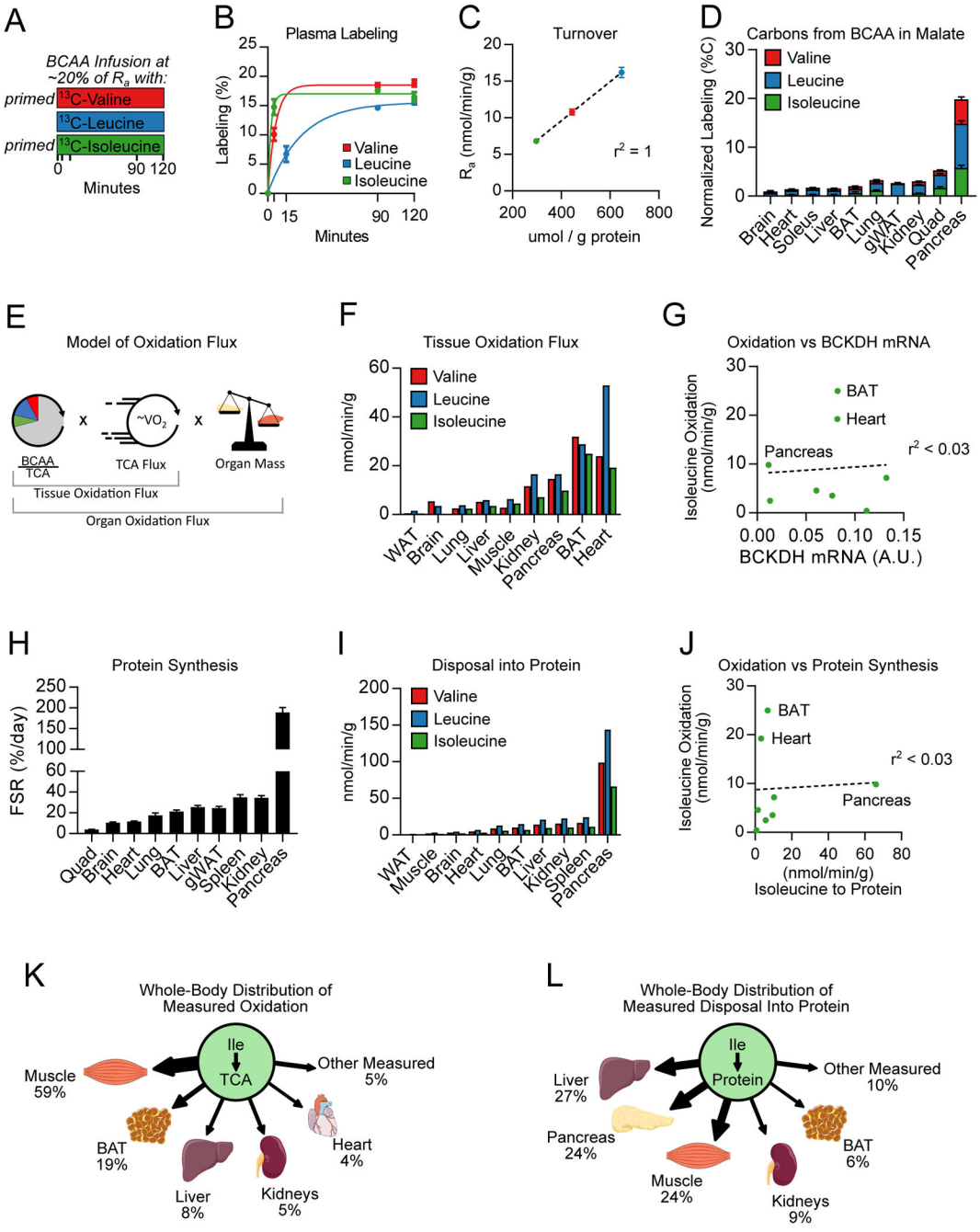


**Figure 2. Integrated quantitative analysis of whole-body BCAA disposal.**

(A) Experimental scheme. Mice received a constant intravenous infusion of BCAAs (one labeled with $^{13}C$ and the other two unlabeled). (B) Constant infusion achieves isotopic steady state. Data show labeling (%) of the indicated labeled BCAAs in plasma. (C) Perfect correlation between the content of each BCAA in protein and the rate of appearance ($R_a$) of each BCAA. (D) % of labeled carbons in malate in the indicated tissues, normalized to the % of label in plasma BCAAs. Labeled carbons refer to the sum of all labeled forms, with each form weighted by fraction of carbon atoms labeled. (E and F) Schematic model (E) and data (F) of tissue BCAA oxidation flux, calculated from the TCA labeling fraction from

BCAAs and TCA turnover flux inferred from tissue oxygen consumption rate ($VO_2$). See Methods for details. (G) Lack of correlation between isoleucine oxidation flux and BCKDHA mRNA levels in each tissue. (H and I) Fractional synthesis rate (FSR) of proteins from BCAAs and calculated disposal flux into proteins in each tissue (I). (J) Lack of correlation between isoleucine oxidation and disposal to proteins in each tissue. (K and L) Schematic of tissue distribution of isoleucine oxidation (K) and disposal into protein (L) in healthy mice. N = 5, 8, and 5 for $^{13}$C-valine, $^{13}$C-leucine and $^{13}$C-isoleucine infusions, respectively. Data are means and error bars are ± SE. See also Figure S2.

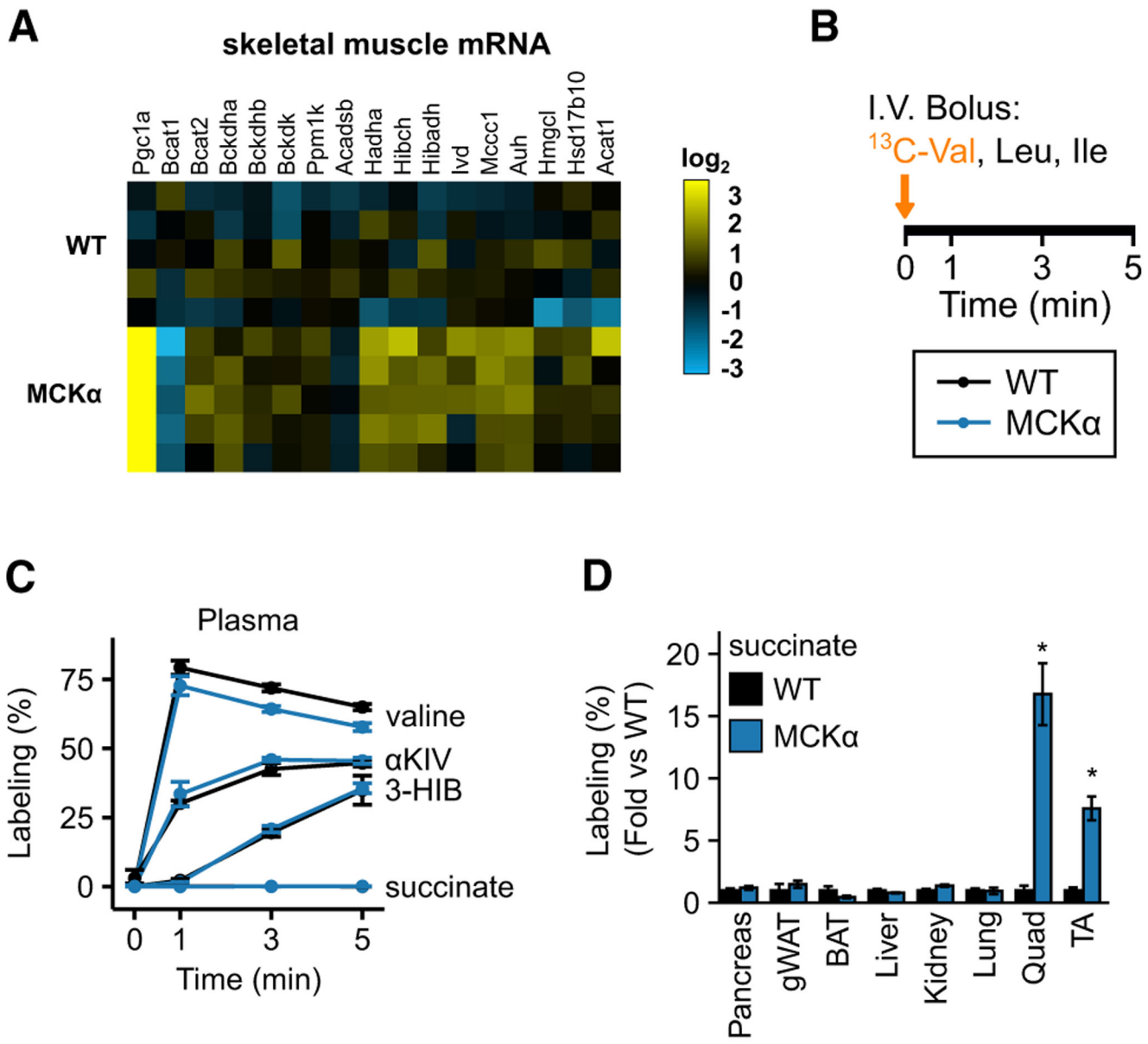


**Figure 3. Transcriptional regulation of BCAA oxidation.**

(A) Transgenic expression of PGC-1α in skeletal muscle induces BCAA catabolic genes. Heat map shows gene expression levels of BCAA oxidation enzymes in skeletal muscle in wild-type (WT) and PGC-1α muscle-specific transgenic mice (MCKα). N = 5. (B) Experimental scheme. Mice received an intravenous bolus injection of [U-$^{13}$C]-valine with unlabeled leucine and isoleucine. Blood was collected at 1, 3, 5 min, and tissues were harvested at 5 min. (C) Plasma labeling (%) of the indicated metabolites. N = 3 and 4 for WT and MCKα, respectively. (D) BCAA oxidation is increased in skeletal muscle of MCKα mice. Data show labeled carbons in succinate in the indicated tissues normalized to WT. Data are means and error bars are ± SE. *$p$<0.05 by Student's $t$-test. See also Figure S3.

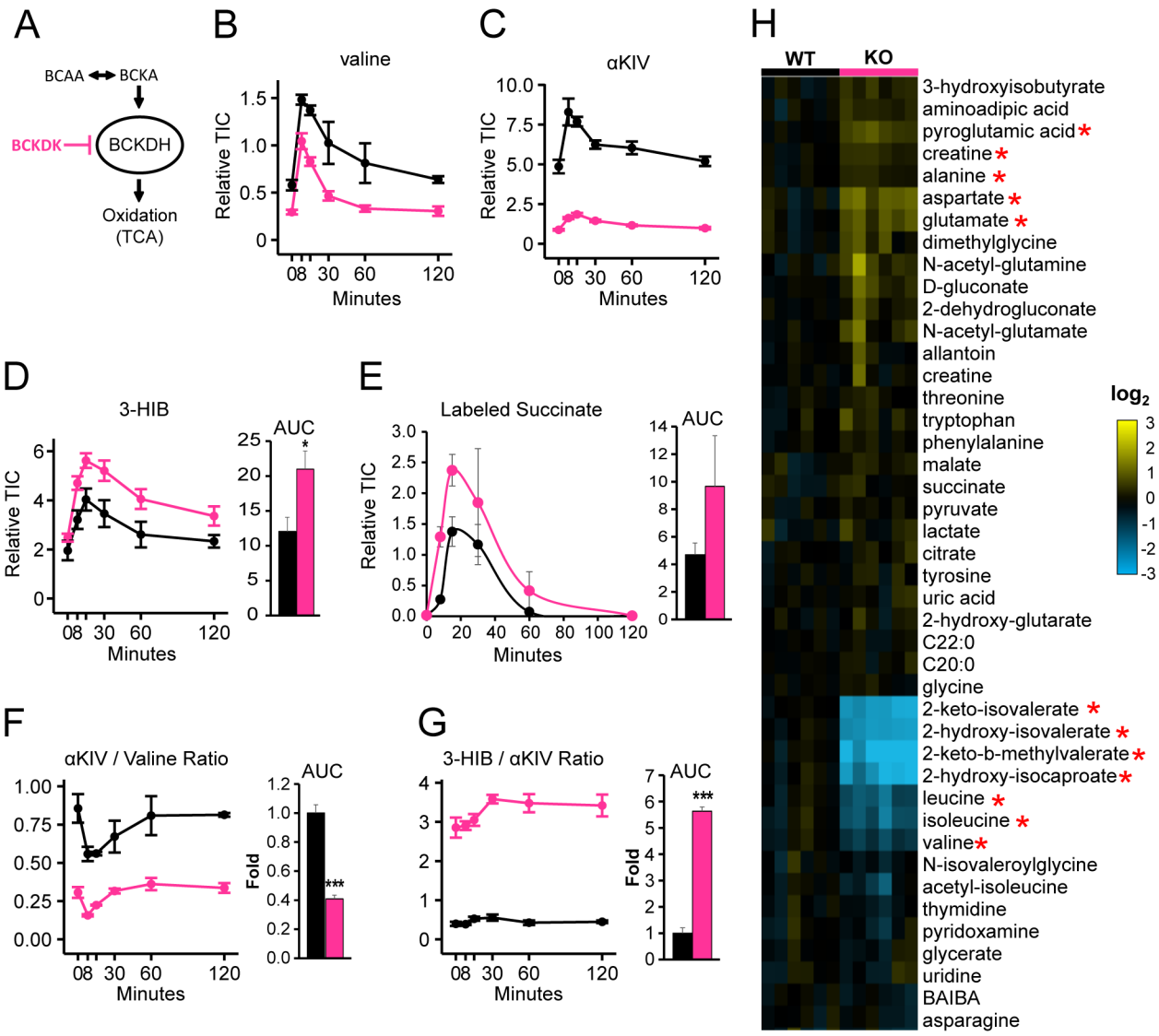


**Figure 4. Whole body BCKDK deletion increases systemic BCAA oxidation and establishes new metabolic steady states.**

(A) Schematic of BCKDK-mediated regulation of BCAA oxidation. (B-D) Plasma levels of the indicated metabolites after oral gavage with [U-$^{13}$C]-isoleucine and unlabeled leucine and valine in control (WT, black) and BCKDK KO (pink) mice. TIC, total ion counts. Bar graph in D shows changes in area under curve (ΔAUC) from the base line (time 0). (E) BCKDK deletion increases systemic BCAA oxidation. Data show total labeled carbons in plasma succinate. (F and G) BCKDK deletion establishes new metabolic steady states. Data show plasma ratios of αKIV to valine (F) or 3-HIB to αKIV (G). (H) Metabolomics heatmap in plasma from WT and BCKDK KO mice. N = 6. Data are means and error bars are ± SE. *$p$<0.05 and ***$p$<0.001 by Student's $t$-test. For the heatmap, FDR correction was performed with $q$<0.05. See also Figure S4.

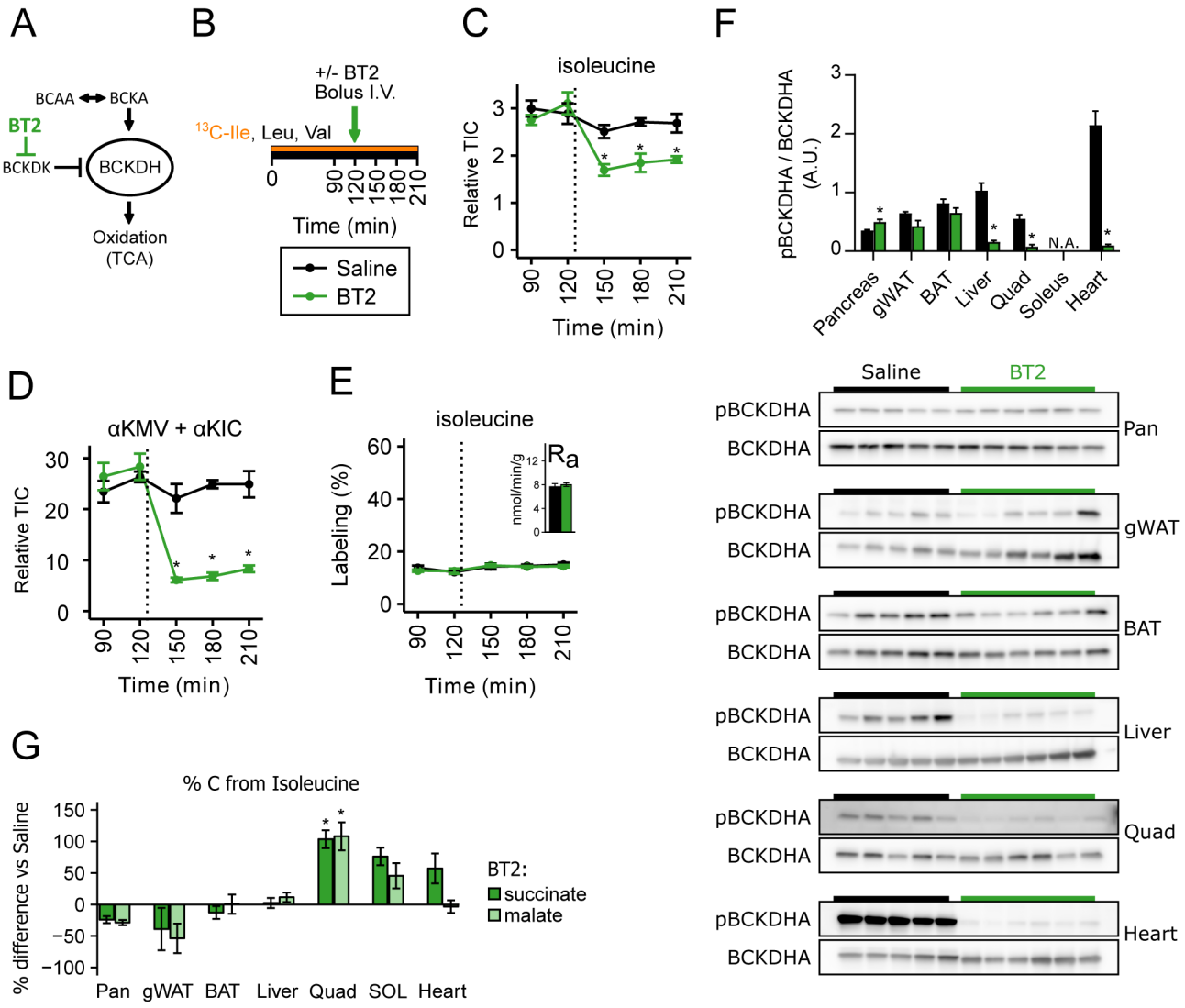


**Figure 5. Acute pharmacological inhibition of BCKDK activates BCAA oxidation specifically in muscle.**

(A) BT2 activates BCAA oxidation by inhibiting BCKDK activity. (B) Experimental scheme. Mice received a constant intravenous infusion of [U-$^{13}$C]-isoleucine with unlabeled leucine and valine for 210 min. At 120min, mice received a bolus injection of vehicle (black) or BT2 (green) during the infusion. (C and D) BT2 acutely reduces plasma levels of isoleucine (C) and BCKAs (D). (E) Plasma labeling (%) of isoleucine. Inset shows calculated isoleucine appearance rate ($R_a$) (F) Western blot analyses of pBCKDHA and total BCKDHA (bottom) and their quantified ratios (top) in the indicated tissues in response to BT2. Soleus samples were not available for these analyses. (G) BT2 specifically activates isoleucine oxidation in skeletal muscle. Data show labeled carbons in the tissue TCA intermediates normalized to the plasma labeled isoleucine, expressed as the percent difference between vehicle and BT2-treated mice. N = 5 and 6 for saline and BT2 groups, respectively. Data are means and error bars are ± SE. *$p$<0.05 by Student's $t$-test. See also Figure S5.

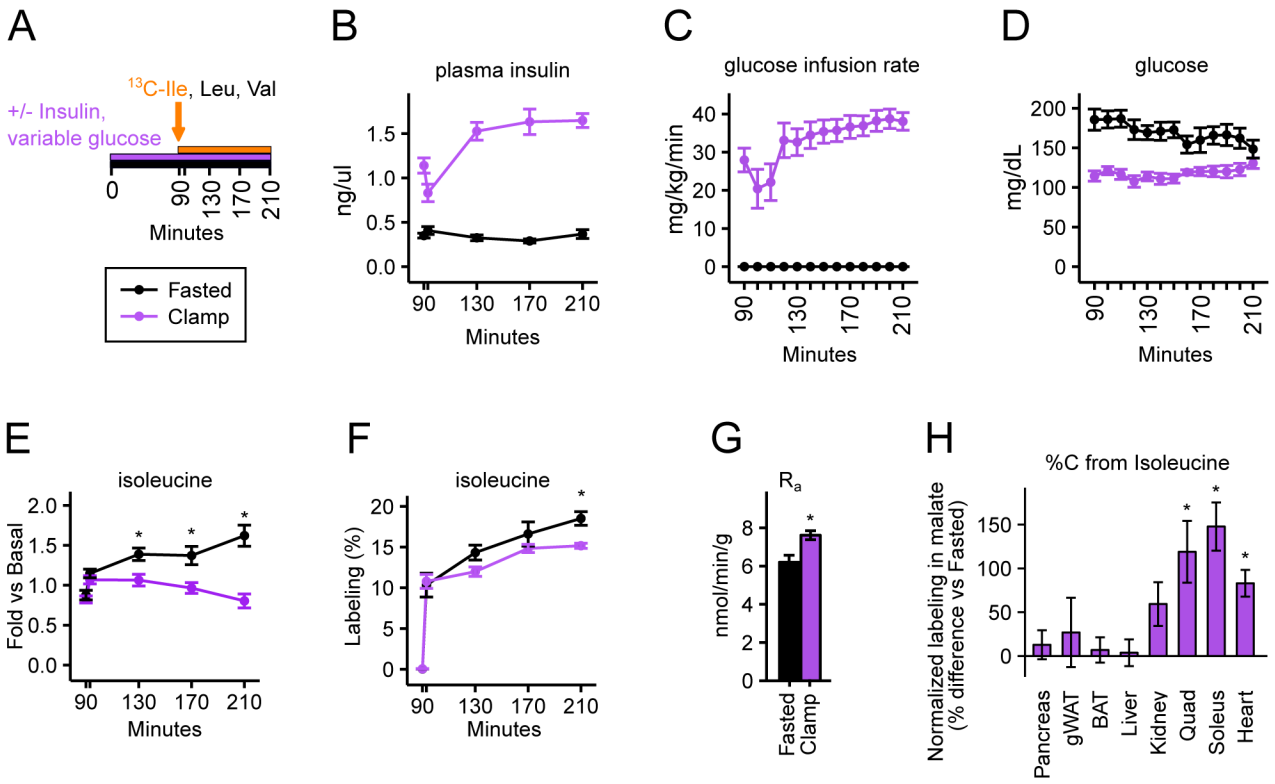


**Figure 6. Insulin acutely induces BCAA oxidation selectively in striated muscle.**

(A) Experimental scheme. After hyperinsulinemic-euglycemic clamp for 90 min, mice received a primed-constant infusion of [U-$^{13}$C]-isoleucine with unlabeled leucine and valine for additional 120 min. Blood was collected at 0, 90, 93, 130, 170, and 210 min, and tissues were harvested at 210 min. (B-D) Vehicle (black) or insulin (purple) was constantly infused to achieve hyperinsulinemic state (B). Glucose was also infused (C) to achieve euglycemic state (D). (E-G) Insulin reduces plasma BCAA levels (E) and slightly increases endogenous isoleucine release from proteolysis (F and G). (H) Insulin stimulates isoleucine oxidation specifically in striated muscle. Data show labeled carbons in the tissue malate normalized to the plasma labeled isoleucine, expressed as the percent difference between vehicle and insulin-treated mice. N = 9 and 10, respectively. Data are means and error bars are ± SE. *$p$<0.05 by Student's $t$-test. See also Figure S6.

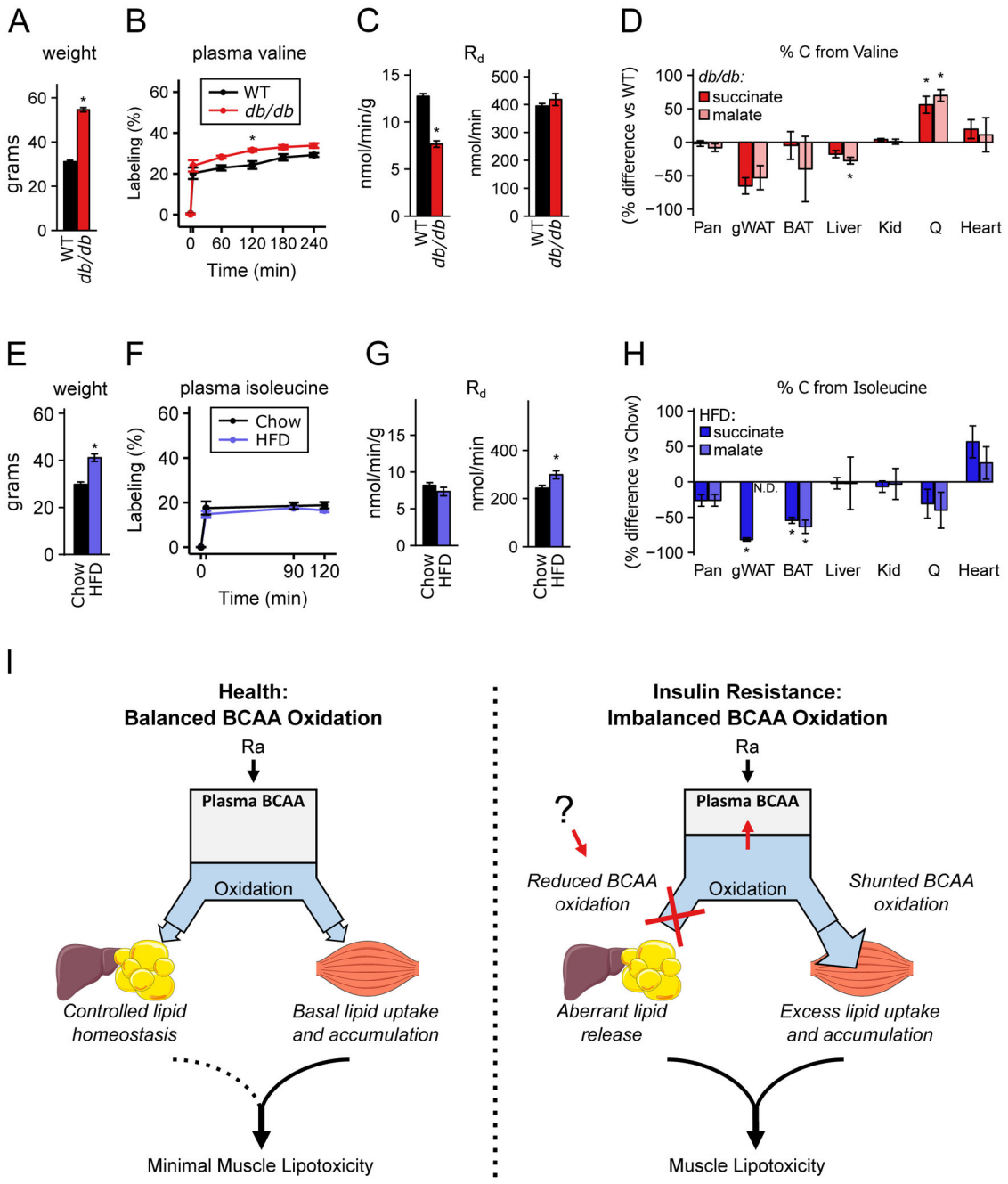


**Figure 7. Obese and diabetic mice redistribute whole-body BCAA oxidation.**

(A) *db/db* mice have doubled body weight compared to the littermate control (WT). (B) Plasma labeling (%) of valine, after constant infusion of [U-$^{13}$C]-valine with unlabeled leucine and isoleucine at the rate adjusted to total blood volume. (C) *db/db* mice show reduced capacity of valine disposal. Data show valine disposal rate ($R_d$) per g body weight (left) or total (right). (D) *db/db* mice show altered valine oxidation preference in multiple tissues. Data show labeled carbons in the tissue TCA intermediates normalized to the plasma labeled valine, expressed as the percent difference between control and *db/db* mice. N = 7 and 8 for control and *db/db* mice, respectively. (E) HFD increases body weight. (F) Plasma

labeling (%) of isoleucine, after constant infusion of [U-$^{13}$C]-isoleucine with unlabeled leucine and valine. (G) Mice fed HFD show normal capacity of valine disposal. Data show valine disposal rate ($R_d$) per g body weight (left) or total (right). (H) Mice fed HFD show reduced valine oxidation preference in adipose tissues. Data show labeled carbons in the tissue TCA intermediates normalized to the plasma labeled isoleucine, expressed as the percent differences between chow and HFD-fed mice. N = 5 and 6 for Chow and HFD groups, respectively. Data are means and error bars are ± SE. *$p$<0.05 by Student's $t$-test. (I) Proposed model of casual relationship between altered tissue BCAA oxidation and elevated circulating BCAA levels in insulin resistance. In healthy conditions (left), BCAA oxidation is balanced among different organs. Genetic and environmental factors suppress BCAA oxidation in the liver and adipose tissues (right), causing increased circulating BCAA levels and overflow of BCAAs into skeletal muscle, resulting in lipotoxicity and insulin resistance. See text for details. See also Figure S7.

## KEY RESOURCES TABLE

| REAGENT or RESOURCE | SOURCE | IDENTIFIER |
|---|---|---|
| Antibodies | | |
| BCKDK | Sigma | Cat# HPA017995; RRID:AB_1845309 |
| pBCKDHA | Bethyl | Cat# A304-672A; RRID:AB_2620867 |
| BCKDHA | Bethyl | Cat# A303-790A; RRID:AB_11218185 |
| Chemicals, Peptides, and Recombinant Proteins | | |
| [U-$^{13}$C]-valine | Cambridge Isotopes | Cat# CLM-2249-H |
| [U-$^{13}$C]-leucine | Cambridge Isotopes | Cat# CLM-2262-H |
| [U-$^{13}$C]-isoleucine | Cambridge Isotopes | Cat# CLM-2248-H |
| [U-$^{13}$C]-αKIV | Cambridge Isotopes | Cat# CLM-4418 |
| BT2 (3-Chloro-benzo[b]thiophene-2-carboxylic acid) | Sigma | Cat# 592862; CAS# 21211-22-3 |
| PhosSTOP phosphatase inhibitor | Roche | Cat# 4906845001 |
| Complete miniproteinase inhibitor | Roche | Cat# 5892970001 |
| AEBSF | Sigma | Cat# A8456 |
| Aprotinin | Sigma | Cat# A6279 |
| Bestatin | Sigma | Cat# B8385 |
| E-64 | Sigma | Cat# E3132 |
| Leupeptin Hemisulfate | Sigma | Cat# L2884 |
| Pepstatin A | Roche | Cat# P5318; CAS# 26305-03-3 |
| NaF | Sigma | Cat# S7920 |
| $Na_3VO_4$ | Sigma | Cat# 450243 |
| XBridge BEH Amide XP column | Waters | Cat# 176002889 |
| Poroshell 120 EC-C18 column | Agilent | Cat# 693775-902 |
| Critical Commercial Assays | | |
| Mouse Insulin ELISA | Crystal Chem | Cat# 90080 |
| Experimental Models: Organisms/Strains | | |
| Mouse: WT: C57blk6J | The Jackson Laboratory | JAX# 000664 |
| Mouse: BCKDK KO | Joshi et al., 2006 | |
| Mouse: MCKα | Lin et al., 2002 | JAX# 008231 |
| Mouse: *db/db* | The Jackson Laboratory | JAX# 000642 |
| Oligonucleotides | | |
| Primers used for qPCR, see Table S4. | Jang et. al, 2016 | N/A |
| Software and Algorithms | | |
| MAVEN Software | Melamud et al., 2010 | http://genomics-pubs.princeton.edu/mzroll/index.php |
| GraphPad Prism 7 | GraphPad Software | https://www.graphpad.com/ |
| Other | | |
| Normal Chow Diet | LabDiet | Cat# 5001 |
| High-Fat Diet | Research Diets | Cat# D12451 |